

1 **Iron budgets for three distinct biogeochemical sites around**  
2 **the Kerguelen archipelago (Southern Ocean) during the**  
3 **natural fertilisation study KEOPS-2**

4  
5 **Andrew R. Bowie<sup>1,2,3</sup>, Pier van der Merwe<sup>1</sup>, Fabien Qu  rou  <sup>1,2,3</sup>, Tom Trull<sup>1,4</sup>,**  
6 **Marion Fourquez<sup>2,5</sup>, Fr  d  ric Planchon<sup>3</sup>, G  raldine Sarthou<sup>3</sup>, Fanny Chever<sup>3,\*</sup>,**  
7 **Ashley T. Townsend<sup>6</sup>, Ingrid Obernosterer<sup>5</sup>, Jean-Baptiste Sall  e<sup>7,8,9</sup>, St  phane**  
8 **Blain<sup>5</sup>**

9 [1] {Antarctic Climate and Ecosystems Cooperative Research Centre (ACE CRC), Private  
10 Bag 80, Hobart, Tasmania, Australia}

11 [2] {Institute for Marine and Antarctic Studies (IMAS), University of Tasmania, Private Bag  
12 129, Hobart, Tasmania, Australia}

13 [3] {Laboratoire des Sciences de l'Environnement Marin (LEMAR), UMR6539  
14 UBO/CNRS/IRD/IFREMER, Institut Universitaire Europ  en de la Mer (IUEM), Technopole  
15 Brest Iroise, 29280 Plouzan  , France}

16 [4] {CSIRO Marine and Atmospheric Research, Castray Esplanade, Hobart, Tasmania,  
17 Australia}

18 [5] {Universit   Pierre et Marie, Laboratoire d'Oc  anographie Microbienne (LOMIC), UMR  
19 7621 CNRS UPMC, Avenue du Fontaul  , 66650 Banyuls sur mer, France}

20 [6] {Central Science Laboratory (CSL), University of Tasmania, Private Bag 74, Hobart, TAS  
21 7001, Australia}

22 [7] {Sorbonne Universit  s, UPMC Univ., Paris 06, UMR 7159, LOCEAN-IPSL, F-75005,  
23 Paris, France}

24 [8] { CNRS, UMR 7159, LOCEAN-IPSL, F-75005, Paris, France}

25 [9] {British Antarctic Survey, High Cross, Cambridge, CB3 0ET, United Kingdom}

26 [\*] {now at: National Oceanography Centre, University of Southampton Waterfront Campus,  
27 European Way, Southampton SO14 3ZH, United Kingdom }

28 Correspondence to: A. R. Bowie (Andrew.Bowie@utas.edu.au)

29

## 1 **Abstract**

2 Iron availability in the Southern Ocean controls phytoplankton growth, community  
3 composition and the uptake of atmospheric CO<sub>2</sub> by the biological pump. The KEOPS-2  
4 project, a GEOTRACES ‘Process Study’, took place around the Kerguelen plateau in the  
5 Indian sector of the Southern Ocean. This is a region naturally fertilised with iron at the scale  
6 of hundreds to thousands of square kilometres, producing a mosaic of spring blooms which  
7 show distinct biological and biogeochemical responses to fertilization. This paper presents  
8 biogeochemical iron budgets (incorporating vertical and lateral supply, internal cycling, and  
9 sinks) for three contrasting sites: an upstream high-nutrient low-chlorophyll reference, over  
10 the plateau, and in the offshore plume east of Kerguelen Island. These budgets show that  
11 distinct regional environments driven by complex circulation and transport pathways are  
12 responsible for differences in the mode and strength of iron supply, with vertical supply  
13 dominant on the plateau and lateral supply dominant in the plume. Iron supply from ‘new’  
14 sources (diffusion, upwelling, entrainment, lateral advection, atmospheric dust) to surface  
15 waters of the plume was double that above the plateau and 20 times greater than at the  
16 reference site, whilst iron demand (measured by cellular uptake) in the plume was similar to  
17 the plateau but 40 times greater than the reference. ‘Recycled’ iron supply by bacterial  
18 regeneration and zooplankton grazing was a relative minor component at all sites (<8% of  
19 ‘new’ supply), in contrast to earlier findings from other biogeochemical iron budgets in the  
20 Southern Ocean. Over the plateau, a particulate iron dissolution term of 2.5% was invoked to  
21 balance the budget; this approximately doubled the standing stock of dissolved iron in the  
22 mixed layer. The exchange of iron between dissolved, biogenic particulate and lithogenic  
23 particulate pools was highly dynamic in time and space, resulting in a decoupling of iron  
24 supply and carbon export and, importantly, controlling the efficiency of fertilization.

25

## 26 **1 Introduction**

27 The concentration of carbon dioxide in earth’s atmosphere and therefore earth’s climate is  
28 highly sensitive to modification of the marine carbon (C) cycle due to the growth of  
29 phytoplankton in the Southern Ocean (Sarmiento and Gruber, 2006). These single-cell plants  
30 remove inorganic carbon from surface seawater during photosynthesis, which can be directly  
31 transferred into the deep sea when they die and sink, or indirectly through the food web. The  
32 Southern Ocean is responsible for 30% of global ocean carbon export (Schlitzer, 2002). As

1 first demonstrated over 20 years ago, phytoplankton growth in the Southern Ocean is limited  
2 by the availability of the micro-nutrient trace element iron (Fe; Martin, 1990). Low dissolved  
3 iron (dFe) availability limits the annual uptake of atmospheric carbon dioxide (CO<sub>2</sub>) by the  
4 Southern Ocean (Boyd et al., 2000), shapes phytoplankton species composition and  
5 physiology (Assmy et al., 2013), the cycling of other nutrient elements (Moore and Doney,  
6 2007) and thus the structure of the entire marine ecosystem (Boyd and Ellwood, 2010).

7 Artificial mesoscale ocean iron fertilisation experiments have unequivocally demonstrated the  
8 role of Fe in setting phytoplankton productivity, biomass and community structure in high  
9 nutrient low chlorophyll (HNLC) regions (de Baar et al., 2005; Boyd et al., 2007). However,  
10 the ‘carbon sequestration efficiency’ of ocean fertilisation as a means to sequester  
11 atmospheric CO<sub>2</sub> (calculated as the additional (net) C that is exported from surface waters into  
12 the deep (>1000 m) ocean for a given addition of Fe) varies widely between experiments and  
13 is considerably less than estimates from the early iron fertilisation experiments (see discussion  
14 in de Baar et al., 2008). This is due to a number of factors, including rapid grazing of  
15 phytoplankton in surface waters, loss of added Fe by its precipitation and scavenging onto  
16 sinking particles, differences in estimated or assumed Fe/C ratios of the cells, and changes in  
17 wind mixed layer depth.

18 The natural resupply of iron to Fe-depleted waters is a more efficient process (Blain et al.,  
19 2007), although in part this depends on the mode of Fe delivery (e.g., from above, laterally or  
20 from below), the ability of organic ligands to keep the supplied Fe in solution (Gerringa et al.,  
21 2008), and for continued ocean fertilisation is in part reliant on the concurrent supply of other  
22 major nutrients. In the Indian sector of the subantarctic Southern Ocean, natural Fe supply  
23 from the Kerguelen plateau (Blain et al., 2007) and Crozet Islands (Pollard et al., 2009)  
24 results in increased phytoplankton biomass during summer, with chlorophyll levels increasing  
25 to more than an order of magnitude above background; as revealed by NASA MODIS  
26 satellite chlorophyll climatology for January (2003-2010) (Westberry et al., 2013). Previous  
27 research of blooms in these localised ‘natural laboratories’ have provided invaluable insights  
28 into mechanisms linking iron fertilisation and carbon cycling in the Southern Ocean,  
29 especially since they can address the effects of persistent, varying and multiple Fe sources  
30 that are not accessible through deliberate artificial mesoscale fertilisation experiments.

31 The KEOPS-1 (KErguelen: compared study of Ocean and Plateau in Surface waters) project  
32 which took place in the late austral summer of January – February 2005 demonstrated that

1 this natural fertilisation of the Southern Ocean resulted in dramatic changes in the functioning  
2 of the ecosystem with large impacts on marine biogeochemical cycles (Blain et al., 2007,  
3 2008a). These observations of the bloom were largely confined to the plateau region, where  
4 vertical upwelled supply from the plateau sediments (Blain et al., 2008b; Zhou et al., 2014)  
5 and lateral advection of water that had been in contact with the continental shelf of Heard  
6 Island to the south (Chever et al., 2010), were the dominant sources of dissolved and  
7 particulate Fe (as confirmed using REE and Ra isotope tracers; van Beek et al., 2008; Zhang  
8 et al., 2008). The interaction of waters, islands and plateau of the Kerguelen archipelago with  
9 several circumpolar fronts of the Southern Ocean allowed us to make a first attempt at placing  
10 our regional KEOPS-1 observations within a broader basin scale context (Blain et al., 2007).

11 The KEOPS-2 project was designed to improve the spatial and temporal coverage of the  
12 Kerguelen region. During KEOPS-2, which was approved as a GEOTRACES Process Study<sup>1</sup>,  
13 we studied the region above and downstream of the plateau and observed a massive natural  
14 iron fertilisation at the scale of hundreds of thousands of square kilometres. This produced a  
15 patchwork of blooms with diverse biological and biogeochemical responses, as detailed in the  
16 multiple studies in this special issue of Biogeosciences (volume 11). KEOPS-2 was also  
17 carried out in the austral spring to document the early stages of the bloom and to complement  
18 results of KEOPS-1 obtained in late summer during the start of the decline of the bloom, with  
19 a principal aim to better constrain the mechanism of Fe supply to surface waters earlier in the  
20 season.

21 Since Fe is actively taken up into phytoplankton, and transferred throughout the food-web,  
22 including removal by particle settling and remineralisation in deep waters, the assessment of  
23 its availability is quite complex and cannot be judged from dFe levels in surface waters alone  
24 (Breitbarth et al., 2010). Advances in chemical oceanographic techniques for trace elements  
25 through the GEOTRACES program (SCOR Working Group, 2007) now allow the  
26 measurement of Fe associated with different phases (dissolved and particulate), internal  
27 biological recycling and Fe export from surface waters. The results from earlier iron  
28 biogeochemical budgets for FeCycle-I (Boyd et al., 2005; Frew et al., 2006), KEOPS-1 (Blain  
29 et al., 2007; Chever et al., 2010), CROZEX (Planquette et al., 2007, 2009) and SAZ-Sense  
30 (Bowie et al., 2009) have highlighted that the dominant 'new' Fe fluxes are associated with

---

<sup>1</sup> <http://www.geotraces.org/cruises/cruise-summary/68-science/process-studies/206-geotraces-process-studies>

1 the particulate phase. Particles thus represent an important transport vector for trace metals in  
2 the marine ecosystem, although their bioavailability or transfer into a bioavailable fraction  
3 remains uncertain. Suspended particles have also been shown to be important aspects of  
4 sedimentary, boundary layer Fe sources and export processes (Tagliabue et al. 2009; Homoky  
5 et al., 2013; Marsay et al., 2014; Wadley et al., 2014), with particles being transported  
6 laterally over hundreds of kilometres in the ocean (Lam et al., 2006; Lam and Bishop, 2008).  
7 The biological cycling of particulate Fe may therefore be the most important aspect of the  
8 complete Fe biogeochemical cycle especially since earlier budgets have demonstrated that  
9 biological Fe ‘demand’ cannot be satisfied by the ‘new’ Fe supply (Boyd et al., 2005; Blain et  
10 al., 2007; Sarthou et al., 2008; Bowie et al., 2009; de Jong et al., 2012). A simple one  
11 dimensional vertical model that correctly represented the input of dFe to surface waters  
12 during KEOPS-1 did not accurately represent the supply of other geochemical tracers or  
13 particulate Fe (Blain et al., 2007; van Beek et al., 2008; Zhang et al., 2008), and the role of  
14 dissolved and particulate Fe earlier in the season (winter stock) in the Kerguelen region has  
15 yet to be quantified.

16 This paper presents a short-term (days-weeks) Fe budget for the period of the KEOPS-2 study  
17 for each of three process sites: (i) a “Plateau” bloom site (A3) on the central Kerguelen  
18 plateau studied during late summer on KEOPS-1 and reoccupied during spring on KEOPS-2;  
19 (ii) a “Plume” bloom site (E) east of Kerguelen Island which was located within a quasi-  
20 stationary, bathymetrically trapped recirculation feature near the Polar Front; and (iii) a  
21 “Reference” site (R-2) south of the Polar Front (PF) and upstream (southwest) of Kerguelen  
22 in HNLC waters. We focus on mixed layer integrated pools of dissolved Fe and particulate Fe  
23 (which we further separate into biogenic and lithogenic fractions using elemental  
24 normalisers), estimate the fluxes of Fe associated with ‘new’ and ‘recycled’ Fe sources, and  
25 compare Fe supply and demand with implications for bloom duration and magnitude. Our  
26 observations also include particulate measurements in both suspended water column (in situ  
27 pump; ‘ISP’) and sinking export (free-floating sediment trap; ‘P-trap’) particles below the  
28 mixed layer, with linkage to food web processes via discussion of iron-to-carbon (Fe/C)  
29 ratios. Finally, we present a seasonal comparison of our springtime budget for KEOPS-2 with  
30 late summer observations from KEOPS-1, and also make comparison with findings from  
31 other sectors of the Southern Ocean subjected to natural Fe fertilisation (e.g., Frew et al.  
32 (2006) and Boyd et al. (2005) for ‘FeCycle-I’, and Ellwood et al. (2014) for ‘FeCycle-II’ east  
33 of New Zealand; Bowie et al. (2009) for ‘SAZ-Sense’ south of Tasmania; Planquette et al.

1 (2011) for ‘CROZEX’ near the Crozet Islands; and Zhou et al. (2010) for ‘Blue Water Zone’  
2 near the western Antarctic Peninsula). The observations of dFe (Qu  rou   et al., 2015) and  
3 particulate trace metals (van der Merwe et al., 2015) are detailed in companion papers in this  
4 special issue, to allow the current paper to focus explicitly on construction of iron budgets;  
5 however the three papers should be seen as a collective whole.

6

## 7 **2 Material and methods**

### 8 **2.1 Study area**

9 The KEOPS-2 (KErguelen: compared study of Ocean and Plateau in Surface waters)  
10 expedition was carried out in the Indian sector of the Southern Ocean in the vicinity of the  
11 Kerguelen plateau between 7 October and 30 November 2011 on the M.D. *Marion Dufresne*  
12 (Figure 1a). The plateau of the Kerguelen archipelago is a northwest-southeast seafloor  
13 feature approximately 500 m deep and is constrained by the Kerguelen Islands to the north  
14 and the smaller volcanic Heard/McDonald Islands to the south. Our study was conducted in  
15 early austral spring when phytoplankton biomass was developing rapidly and forming a  
16 mosaic of phytoplankton blooms in the region (Trull et al., 2015; Lasbleiz et al., 2014). Since  
17 sampling at the different stations took place at different times over the ~7 week study, our  
18 observations also provide a temporal sequence relative to the development of surface  
19 biomass.

20 The Kerguelen bloom has two main features, a northern branch that extends northeast of the  
21 island into waters both south and north of the PF, and a larger bloom covering ~45,000 km<sup>2</sup>  
22 south of the PF and largely constrained to the shallow bathymetry of the Kerguelen plateau  
23 (<700m) (Mongin et al., 2008; Supplementary Material in Trull et al., 2015) (Figures 1(b) and  
24 2). Thirty-two stations were sampled during KEOPS-2, often with repeat visits. Here we focus  
25 on three study sites, namely: plateau A3, plume E and reference R-2 (Figure 1). Two visits  
26 were made to A3 at the start (A3-1) and end (A3-2) of the voyage (28 days apart), and five  
27 visits were made to site E (over 21 days) to document the bloom development. Based on the  
28 trajectories of surface drifters, stations E-1, E-3 and E-5 were taken as tracking the middle of  
29 a recirculation region (d'Ovidio et al., 2015), so that they can be considered as pseudo-  
30 Lagrangian and their succession in time can be considered a first order time series. Full details  
31 of other stations and sampling designed to document the meridional and zonal extensions of

1 the blooms on the plateau and to the east of Kerguelen are contained in companion papers in  
2 this special issue of Biogeosciences.

3 The hydrology and circulation around and above the Kerguelen plateau have been described  
4 by Park et al. (2008a, 2008b, 2014a), van Beek et al. (2008), Zhang et al. (2008) and Zhou et  
5 al. (2014). The mean circulation is shown in Figure 1(b). Briefly, the Kerguelen plateau  
6 constitutes a barrier to the eastward flowing Antarctic Circumpolar Current (ACC), the main  
7 jets of which are the Sub-Antarctic Front (SAF) and PF. Most of the ACC is deflected north  
8 of the Kerguelen Islands as Sub-Antarctic Surface Water (SASW) but some filaments pass  
9 between the Kerguelen Islands and Heard Island (as the PF) and further south between Heard  
10 Island and Antarctica (Roquet et al., 2009). Above the plateau, the remainder of the ACC  
11 comes from the western part of the plateau. Currents of AASW travelling along the western  
12 flank of the plateau are deflected south and east of Heard Island as a branch of the Fawn  
13 Trough Current (FTC) (Sokolov and Rintoul, 2009), before travelling in a broadly northwest  
14 direction up along the eastern shelf-break. The water flow is then deflected toward the east of  
15 Kerguelen Island, where there is an intense mixing zone consisting of mesoscale eddies which  
16 travel many thousands of kilometres in the ACC towards the Australian sector of the Southern  
17 Ocean.

18

## 19 **2.2 Sampling**

20 All trace metal sampling and analytical procedures followed recommended protocols in the  
21 cookbook<sup>2</sup> published by the international program GEOTRACES (Bishop et al., 2012; Cutter  
22 and Bruland, 2012; Planquette and Sherrell, 2012). All methods have been successfully used  
23 previously by this team during the KEOPS-1 (Blain et al., 2008b) and SAZ-Sense projects  
24 (Bowie et al., 2009). Subtle differences in methods employed during the earlier KEOPS-1 and  
25 SAZ-Sense projects are described in those papers and/or later in this manuscript.

26

---

<sup>2</sup> <http://www.geotraces.org/libraries/documents/Intercalibration/Cookbook.pdf>

## 1 **2.2.1 Trace metal rosette (TMR)**

2 Water column samples were collected using 10 L externally-closing, Teflon-lined Niskin-  
3 1010X bottles deployed on an autonomous 1018 intelligent rosette system ('TMR', specially  
4 adapted for trace metal work, General Oceanics Inc.). The polyurethane-powder-coated  
5 aluminium rosette frame was suspended on Kevlar rope which passed through a clean block  
6 with a plastic sheave (General Oceanics) and was lowered to a maximum depth of 1300 m.  
7 Bottles were tripped at pre-programmed depths using a pressure sensor as the TMR was being  
8 raised through the water column at approximately  $0.5 \text{ m s}^{-1}$ .

9 All sample processing was carried out under an ISO class 5 trace-metal-clean laminar flow  
10 bench in a HEPA filtered-air clean container, with all materials used for sample handling  
11 thoroughly acid-washed. Samples were drawn through C-Flex tubing (Cole Parmer) and  
12 filtered in-line through  $0.2 \text{ }\mu\text{m}$  pore-size acid-washed capsules (Pall Supor membrane  
13 Acropak 200 or Sartorius Sartobran 300 filters). The dissolved fraction is thus likely to  
14 contain colloids and small particles  $<0.2 \text{ }\mu\text{m}$  in diameter (Bowie and Lohan, 2009). All  
15 transfer tubes, filtering devices and sample containers were rinsed liberally with sample  
16 before final collection in 125 mL Nalgene LDPE bottles. Seawater samples were acidified  
17 within 24 h of collection using 2 mL of concentrated ultrapure hydrochloric acid (HCl,  
18 Seastar BASELINE grade) per L of sample, resulting in an approximate final pH of 1.8,  
19 double bagged and stored for at least 24 h at ambient temperature until analysis.

## 20 **2.2.2 In situ pumps (ISPs)**

21 Suspended particles for trace elemental analysis were collected using 11 large-volume in situ  
22 pumps (McLane Research Laboratories WTS6-1-142LV and Challenger Oceanics pumps),  
23 suspended simultaneously at pre-chosen depths, following methods reported in Bowie et al.  
24 (2009). Up to 2000 L of seawater was filtered across a 142 mm diameter stack (134 mm  
25 diameter active area) consisting of a  $53 \text{ }\mu\text{m}$  nylon pre-filter screen (NYTEX) followed by a  
26 QMA quartz fibre filter ( $1 \text{ }\mu\text{m}$  nominal pore size; Sartorius). The QMA filter was supported  
27 by a  $350 \text{ }\mu\text{m}$  polyester mesh which was placed on top of the Teflon PFA grid of the pump  
28 housing. Prior to use, NYTEX screens were conditioned by soaking in 5%  $\text{H}_2\text{SO}_4$ , rinsed 3x  
29 with Milli-Q grade water, dried at ambient temperature under a laminar flow hood and stored  
30 in clean plastic Ziploc<sup>®</sup> bags. QMA filters were conditioned for trace-metal analysis (pre-  
31 combustion and acid cleaning) following Bowie et al. (2010). Upon recovery of the pumps,



1 sub-samples were taken from the QMA filters using a circular plastic punch (14 mm  
2 diameter) and by cutting the nylon mesh using ceramic scissors. Filters were dried under a  
3 laminar flow bench and stored at -18 °C in acid-washed PCR trays until further analysis in the  
4 home laboratory. The 1-53 µm and >53 µm size fractions were digested and analysed  
5 separately, and the particulate iron (pFe) reported here is the sum of both fractions. The ISPs  
6 were shown to be efficient in capturing large (>53 µm) particles (Planchon et al., 2014).

### 7 **2.2.3 Free-floating traps (P-trap)**

8 Sinking particles for trace elemental analysis were collected using PPS3/3 free-floating  
9 sediment traps (Technicap, France), specially adapted for trace metals, deployed at 200 m.  
10 Traps were deployed for 5.3, 5.1, 1.9 and 1.5 days at stations E-1, E-3, A3-2 and E-5,  
11 respectively. The trap deployed at station R-2 was lost and not recovered. Traps drifted  
12 between 10 and 43 km over the course of the deployment. Full details of the trap deployments  
13 are given in Laurenceau-Cornec et al. (2015) and Planchon et al. (2014). Samples for trace  
14 elemental analysis were collected in three separate acid-washed cups (dedicated for trace  
15 metals) containing a low trace metal brine solution (salinity ~60), each opened for either 1, 3,  
16 8 or 12 h (depending on the station). Upon recovery, cups were taken to a clean room and  
17 particles filtered off-line onto a 47 mm diameter, 2 µm porosity polycarbonate filter under  
18 gentle vacuum using a Teflon PFA unit (Savillex Corp., USA), equipped with a 350 µm pre-  
19 screen (to exclude zooplankton).

20

## 21 **2.3 Analysis**

### 22 **2.3.1 Dissolved iron**

23 Dissolved Fe (dFe) was determined shipboard by flow injection analysis with  
24 chemiluminescence detection (FI-CL) using in-line preconcentration on an 8-  
25 hydroxyquinoline chelating resin (adapted from Obata et al. (1993), de Jong et al. (1998) and  
26 Sarthou et al. (2003)). Dissolved Fe data were quality controlled against the SAFe (“Sampling  
27 and Analysis of Fe”) standard reference materials (Johnson et al., 2007). Full data including  
28 certification results and analytical figures of merit are reported in Quéro   et al. (2015).

### 1 **2.3.2 Particulate iron**

2 Particulate Fe (pFe) was determined as follows. Sampled particles were acid extracted in 1  
3 mL concentrated HNO<sub>3</sub> (Seastar Baseline) for 12 h on a DigiPREP HP Teflon hotplate  
4 supplied with HEPA filtered air (SCP Science) at 120 °C using 15 mL Teflon PFA Savillex  
5 vials. Digest solutions were diluted with 10 mL ultra-high purity water to 10 % HNO<sub>3</sub> and  
6 spiked with 10 ppb indium as internal standard prior to analysis by sector field inductively  
7 coupled plasma mass spectrometry (Finnigan ELEMENT 2, Thermo Scientific), following  
8 Bowie et al. (2010). Blanks from replicate analysis of filters treated identically to the sample  
9 filters, but without large volumes of seawater passed through them, were typically 2-3 % and  
10 <1 % of the pFe sample concentrations for the ISP deployments and P-trap deployments,  
11 respectively. Recoveries from the analysis of the Community Bureau of Reference plankton  
12 certified reference material BCR-414 were excellent, with a 101 % recovery (n=3) for pFe.  
13 Full data are reported in van der Merwe et al. (2015).

### 14 **2.3.3 Particulate organic carbon and nitrogen**

15 For particulate organic carbon (POC) and particulate nitrogen (PN) analyses, QMA quartz  
16 filters from the ISPs were sub-sampled in a flow-bench using a 14 mm diameter plastic punch  
17 and transferred to silver foil cups (Sercon brand p/n SC0037). Samples were also collected  
18 from the P-traps for POC and PN analyses (see Laurenceau-Cornec et al., 2015). Samples  
19 were treated with a 40 µL aliquot of 2 N HCl to remove carbonates (King et al., 1998), dried  
20 at 60 °C for 48 h, and stored in a desiccator until analysis using a Thermo-Finnigan Flash  
21 EA1112 elemental analyzer (using sulfanilamide standards) at the Central Science  
22 Laboratory, University of Tasmania. The >53 µm fraction was treated in the same way at the  
23 Vrije Universiteit Brussel, after first transferring the material from one fourth of the screen  
24 using pre-filtered seawater onto 25 mm diameter, 1.0 µm pore size silver membrane filters  
25 (Sterlitech, Concord). Blank corrections for the pump samples were estimated from filters  
26 prepared identically but not deployed on the ISPs, and for the trap samples by re-filtering the  
27 pre-filtered seawater. All blank corrections were less than 2 % for all samples. The sub-  
28 sampling introduces uncertainties of 5-10 % from inhomogeneous filter coverage that exceeds  
29 the analytical uncertainty of the POC analysis of ~1 % (Trull et al., 2015).

30

## 1 **2.4 Biological iron cycling**

### 2 **2.4.1 Iron uptake**

3 Trace metal clean seawater was collected from the mixed layer (20-40 m) using the TMR,  
4 transferred into acid-washed polycarbonate bottles and 0.2 nmol L<sup>-1</sup> (final concentration) of  
5 enriched <sup>55</sup>Fe as FeCl<sub>3</sub> added (1.83 x 10<sup>3</sup> Ci mol<sup>-1</sup> of specific activity, Perkin Elmer). Bottles  
6 were placed at in situ temperature in on-deck incubators continuously fed by surface seawater.  
7 Incubations were conducted for 24 h (sunrise to sunrise) at several light intensity levels (75,  
8 45, 25, 16, 4, and 1 % of photosynthetically-active radiation; PAR). For stations R-2, A3-1, E-  
9 1 and E-3, seawater was prefiltered on a 25 µm mesh size before <sup>55</sup>Fe was added. After  
10 incubation, 300 mL of seawater was passed through 0.2 µm pore-size nitrocellulose filters (47  
11 mm diameter, Nuclepore). To determine intracellular Fe uptake rates, <sup>55</sup>Fe not incorporated by  
12 cells was removed immediately after filtration using 6 mL of a Ti-citrate-EDTA washing  
13 solution for 2 min., followed by rinsing 3 times with 5 mL of 0.2 µm filtered-seawater for 1  
14 min. (Hudson and Morel, 1989; Tang and Morel, 2006). The filters were placed into plastic  
15 vials and 10 mL of the scintillation cocktail 'Filtercount' (Perkin Elmer) added. Vials were  
16 agitated for 24 hours before the radioactivity on filters was counted with the Tricarb<sup>®</sup>  
17 scintillation counter (precision <10 %). Controls were obtained with 300 mL of microwave-  
18 sterilized seawater (750 W for 5 min.) incubated and treated the same way. Sub-samples for  
19 enumeration by flow cytometry were collected from each bottle just before the filtration step.  
20 Cells were fixed in glutaraldehyde (1 %) and kept frozen (-80 °C) until processing and  
21 analysis. Data were corrected by blank subtraction and Fe uptake rates normalised to the  
22 concentration of Fe in each incubation (in situ dFe and <sup>55</sup>Fe added). Further details are given  
23 in Fourquez et al. (2015).

### 24 **2.4.2 Iron remineralisation**

25 Since iron regeneration was not measured directly by experiment during KEOPS-2, we used  
26 the following approach to calculate iron regeneration fluxes. Bacterial Fe regeneration was  
27 estimated from bacterial turnover times determined from bacterial production and biomass  
28 (Christaki et al., 2014), assuming all loss of bacterial biomass through viral lysis and  
29 flagellate grazing resulted in the regeneration of Fe (Strzepek et al., 2005), and using a  
30 bacterial iron quota of 7.5 µmol Fe (mol C)<sup>-1</sup> (Tortell et al. 1996). The mesozooplankton  
31 grazing contribution to Fe regeneration was assumed to be equal to the experimentally

1 determined Fe regeneration during KEOPS-1 (Sarhou et al., 2008). The regeneration rates  
2 per mesozooplankton individual determined in Sarhou et al. (2008), were then multiplied by  
3 mesozooplankton abundance, calculated from the number of cells captured in a daily haul  
4 over 200 m during KEOPS-2 (Carlotti et al., 2015; values reported in Table 6 in Laurenceau-  
5 Cornec et al., 2015).

6

## 7 **3 Results and Discussion**

### 8 **3.1 Biogeochemical settings at our three study sites**

9 Full descriptions of the dFe and pFe distributions can be found in Qu erou e et al. (2015) and  
10 van der Merwe et al. (2015), respectively, with further presentation of the distributions of  
11 other micronutrient trace elements (Mn, Co, Ni, Cu, Cd, Pb) from KEOPS-2 to be presented  
12 elsewhere. However, briefly our subset of stations used for the iron budgets can be described  
13 as follows.

#### 14 **3.1.1 Reference station R-2**

15 In the upper 100 m, we observed a salinity minimum (33.8) and temperature maximum (2.2  
16  C) characteristic of Antarctic surface water (AASW) overlying a layer of winter water (WW)  
17 at 180-200 m ( $T_{\min}$  of 1.6  C) (Figure 3a). Deeper in the water column, a  $T_{\max}$  of 2.5 C at 500  
18 m (associated with an oxygen minimum; not shown) was indicative of upper circumpolar  
19 deep water (UCDW) overlying a salinity maximum of 34.8 at 1830 m in lower circumpolar  
20 deep water (LCDW). Phytoplankton abundance was low (0.2  $\mu\text{g Chl-a L}^{-1}$ ; Lasbleiz et al.,  
21 2014) and dominated by diatoms, in waters with relatively high surface nitrate concentrations  
22 ( $>25 \mu\text{mol L}^{-1}$ ; Blain et al., 2015), typical of Southern Ocean HNLC conditions (Lasbleiz et  
23 al., 2014).

24 Dissolved Fe concentrations were very low at the surface ( $<0.1 \text{ nmol L}^{-1}$ ) and increased with  
25 depth averaging  $0.3 \text{ nmol L}^{-1}$  in LCDW, broadly tracking the nitrate profile. The pFe profile  
26 showed similar structure to the dFe profile, but with surface and deep water concentrations  
27 between  $0.3$  and  $1.1 \text{ nmol L}^{-1}$  (the deepest sample was 148 m above the seafloor). The  
28 exception was at 500 m where interestingly we observed a dFe and pFe peak of  $0.4$  and  $1.6$   
29  $\text{nmol L}^{-1}$ , respectively. Whilst this maximum may have arisen due to enrichment of Fe in  
30 UCDW delivered from further south, we hypothesise that the Fe supply may have originated

1 from subsurface sediments of the nearby Leclaire Rise (also known as Skiff Bank; Kieffer et  
2 al., 2002), a large seamount which rises to 250 m at 49°50'S 65°00'E (approximately 140 km  
3 northwest of station R-2). Similar lithogenic inputs were also observed for other dissolved  
4 (Mn; Fabien Qu  rou  , pers. comm., data not shown) and particulate (Mn, Al; van der Merwe  
5 et al., 2015) trace elements.

6 The dFe profile at the KEOPS-2 reference station R-2 is similar to the KEOPS-1 reference  
7 station C11 (with the exception of the R-2 enrichment in the 200-700 m depth strata; Figure  
8 4a), noting that the location of C11 was quite different - in HNLC waters to the southeast of  
9 the Kerguelen plateau (51°39'S, 78°00'E) - and we had only 1 dFe data point in UCDW at  
10 C11. In contrast to the similarity of the dFe profiles, the pFe profile at C11 was generally  
11 lower than R-2, with mean values through the water column of  $0.2 \pm 0.14 \text{ nmol L}^{-1}$  (Andrew  
12 Bowie, unpublished data) compared to  $0.53 \pm 0.35 \text{ nmol L}^{-1}$  for station R-2.

### 13 **3.1.2 Plateau station A3**

14 Stations A3-1 (Figure 3b) and A3-2 (Figure 3c) were in relatively shallow waters on the  
15 central plateau, and were impacted by plateau sediments and possibly fluvial and glacial  
16 runoff from basaltic rocks of Heard Island ~300 km upstream (van der Merwe et al., 2015;  
17 Melanie Grenier, pers. comm.). A pycnocline was observed at ~190 m, above which the  
18 salinity (33.9) and nitrate (~29  $\mu\text{mol L}^{-1}$ ) were relatively constant. The mixed layer shoaled  
19 (from 165 to 123 m) and increased in temperature (from 1.7 to 2.2 °C) between the two visits  
20 to A3, consistent with springtime warming of surface waters. We believe the water masses at  
21 A3-1 and A3-2 are comparable since surface waters move slowly in this region (Park et al.,  
22 2008, 2014a; Zhou et al., 2014); this was confirmed by rare earth element (REE) data which  
23 indicated similar waters at both stations marked with fresh continental supplies, only modified  
24 by biological processes (Melanie Grenier, pers. comm.).

25 Surface chlorophyll images revealed that during the 28 days between the first and second  
26 visits to A3, a large diatom spring bloom developed mostly dominated by lightly silicified  
27 *Chaetoceros* spp. (surface Chl-a increasing from 0.2  $\mu\text{g L}^{-1}$  at A3-1 to 1.3  $\mu\text{g L}^{-1}$  at A3-2;  
28 Lasbleiz et al., 2014), which likely resulted in the drawdown of dFe (mean mixed layer values  
29 decreasing from 0.3-0.4  $\text{nmol L}^{-1}$  at A3-1 to 0.1-0.2  $\text{nmol L}^{-1}$  at A3-2). The peak of biomass  
30 had passed by the time we sampled at A3-2, with the bloom starting to fade (Trull et al.,  
31 2015). Below the mixed layer, similar dFe profiles were observed during both visits to A3,

1 with expected significant increases at depth towards the plateau floor (e.g., to 1.30 nmol L<sup>-1</sup> at  
2 480 m at A3-2; note, due to operational constraints, there was no dFe data deeper than 340 m  
3 at A3-1). Such enrichments at depth were also observed in dissolved Mn and Co profiles (F.  
4 Qu  rou  , pers. comm., 2014; data not shown) and dFe profiles from the occupations of station  
5 A3 during the KEOPS-1 study (Fig. 4b), indicative of plateau sedimentary supply.

6 The pFe profiles at A3 showed similar structure to the dFe profile, with lower values at the  
7 surface (<10 nmol L<sup>-1</sup> at A3-1 and <4 nmol L<sup>-1</sup> at A3-2), increasing with depth due to  
8 enrichment from bottom sediments (up to 33 and 14 nmol L<sup>-1</sup> at 440 m at A3-1 and A3-2,  
9 respectively), and were on average 10 times greater than dissolved concentrations through the  
10 water column. The mixed layer pFe concentrations changed remarkably between the two  
11 visits, and the full water column integrated pool was ~70% lower at A3-2 compared to A3-1.  
12 Interestingly, this change was also associated with a shift of particles from the 1-53   m size  
13 range to the >53   m size range, with the larger size class tripling in size (van der Merwe et al.,  
14 2015). The development of the large bloom between our two visits to A3, which consisted of  
15 a diatom community 50-210   m in size (Trull et al., 2015) was likely responsible for  
16 converting the pFe within the surface mixed layer from the smaller size class to the larger size  
17 class. This may have been due to either: (i) physical aggregation of the particles onto diatom  
18 aggregates; and/or (ii) microbially-driven conversion of small lithogenic Fe (1-53   m) to  
19 bioavailable forms and incorporation into the large (>53   m) diatoms as biogenic Fe, with  
20 potentially some fraction of these larger particles exported to depths below the mixed layer, as  
21 previously discussed by Lam et al. (2006), Frew et al. (2006) and Planquette et al. (2011).

22 The spring (Oct-Nov) KEOPS-2 Fe profiles at station A3 showed a similar structure to those  
23 from the late summer (Jan-Feb) KEOPS-1 study, with surface depletion, concentrations  
24 increasing with depth and enrichment just above the plateau seafloor (Figure 4b). Through the  
25 water column, dFe was between 2-5 times greater during KEOPS-2 compared to KEOPS-1  
26 and pFe was ~10 times greater during KEOPS-2 (with the exception of the deepest samples).  
27 The lower values during KEOPS-1 were likely the result of biological uptake in surface  
28 waters and export of Fe during the spring bloom prior to our arrival at the study site,  
29 combined with seasonal changes in the strength of the supply mechanisms to deeper waters at  
30 A3 (discussed in van der Merwe et al., 2015).

### 1 3.1.3 Plume E stations

2 The E stations within the bathymetrically trapped complex recirculation system showed  
3 similar hydrographic and nutrient distributions below the mixed layer (Figures 3d, 3e and 3f),  
4 which shoaled from 64 m at E-1 to 32 m at E-3 to 39 m at E-5, with some internal variability  
5 in water column structure at mid-depths. Surface waters warmed from 2.7 to 3.4 °C between  
6 the occupations of E-1 and E-5, although no significant nitrate drawdown was observed  
7 (Blain et al., 2015). Below AASW, a subsurface temperature minimum ( $T_{\min}$ , ~1.7 °C) was  
8 observed between 180 m (E1) and 220 m (E5), characteristic of WW. The  $T_{\min}$  feature is  
9 associated with waters south of the PF, although the recirculation feature probably also  
10 received SAZ waters mixed in from the north (d'Ovidio et al., 2015). T, S and O<sub>2</sub>  
11 characteristics indicated the presence of UCDW (~600-700 m) and LCDW (deeper than  
12 ~1300 m) deeper in the water column above the seafloor (Qu  rou   et al., 2015). Water parcel  
13 trajectories calculated from altimetry based geostrophic currents indicated that it took  
14 generally >2 months for Fe-rich waters from the plateau to travel to the downstream plume  
15 site associated with the recirculation feature (E stations) (d'Ovidio et al., 2015). However  
16 shorter transport times are also possible due to episodic transport across the PF (Sanial et al.,  
17 2015).

18 Waters at the plume stations showed the largest spatial heterogeneity in surface biomass as  
19 revealed by the evolution of a mosaic of complex blooms seen in satellite images (see  
20 Supplementary Material in Trull et al., 2015). We observed moderate surface Chl-a levels  
21 ranging from 0.3-0.4  $\mu\text{g L}^{-1}$  at E-1 and E-3 to 0.5-0.9  $\mu\text{g L}^{-1}$  at E-5 (Lasbleiz et al., 2014),  
22 noting that as much as 50 % of the chlorophyll was below the mixed layer at the plume  
23 stations due to stratification of the upper water column in the warm, spring conditions. Unlike  
24 the plateau bloom dominated by large cells >53  $\mu\text{m}$ , the community in the plume E stations  
25 was more mixed (Laurenceau-Cornec et al., 2015), with cells present in both the 5-20 and 50-  
26 200  $\mu\text{m}$  size classes (Trull et al., 2015). The E stations showed the highest C export fluxes of  
27 all regions as estimated from Th deficits, nitrate depletions, and free-drifting sediment trap  
28 observations (Planchon et al., 2014; Trull et al, 2015; Laurenceau-Cornec et al., 2015).

29 Due to operational constraints, no dFe data was available at station E-1. The dFe vertical  
30 profiles at E-3 and E-5 were quite different, with a distinct surface enrichment to 0.4  $\text{nmol L}^{-1}$   
31 at E-3 above a minimum of 0.2  $\text{nmol L}^{-1}$  at 100 m. This feature was absent at station E-5,  
32 where dFe was depleted to <0.1  $\text{nmol L}^{-1}$  at the surface, likely due to biological Fe uptake,

1 which was highest at E-5 ( $1745 \text{ nmol m}^{-2} \text{ d}^{-1}$ ) compared to A3-2 ( $1120 \text{ nmol m}^{-2} \text{ d}^{-1}$ ) (Table 1)  
2 and E-4E ( $880 \text{ nmol m}^{-2} \text{ d}^{-1}$ ; data not shown), despite lower POC and primary production (see  
3 discussion below and Fourquez et al., 2015). Deeper in the water column ( $>500 \text{ m}$ ) at E  
4 stations, dFe was broadly uniform ( $0.3\text{-}0.5 \text{ nmol L}^{-1}$ ).

5 The pFe distributions at the three E stations were similar with a surface (35-40 m) enrichment  
6 ( $1.6\text{-}1.9 \text{ nmol L}^{-1}$ ), a minimum at  $\sim 100\text{-}200 \text{ m}$  below the mixed layer ( $0.7\text{-}0.9 \text{ nmol L}^{-1}$ ;  
7 broadly consistent with the  $T_{\text{min}}$  layer), above a maximum at 280-600 m ( $1.7\text{-}2.4 \text{ nmol L}^{-1}$ ),  
8 and with evidence of enrichment near the seafloor at depths  $>1800 \text{ m}$  (up to  $1.5\text{-}2.3 \text{ nmol L}^{-1}$ ).  
9 By applying biogenic (using P) and lithogenic (using Al) normalisers to the data (see  
10 ‘Construction of iron budgets’ section below), surface pFe enrichment was roughly equally  
11 composed of biogenic and lithogenic Fe, whilst the 300-600 m maximum was predominantly  
12 composed of lithogenic Fe ( $>100$ -fold greater than biogenic Fe at these depths). This  
13 lithogenic Fe was most likely from waters enriched from sediments and transported laterally  
14 eastward off the Kerguelen plateau which sits at  $\sim 530 \text{ m}$  below the sea surface. There was no  
15 obvious change in pFe in surface or deep waters during the bloom evolution at the pseudo-  
16 Lagrangian E stations.

17 The KEOPS-1 study only occupied one station in the plume east of Kerguelen (A11 at  
18  $49^{\circ}09'S$   $74^{\circ}00'E$ ). Dissolved Fe at A11 ranged from  $0.09 \text{ nmol L}^{-1}$  at the surface to  $0.17 \text{ nmol}$   
19  $\text{L}^{-1}$  at 1500 m (Blain et al., 2008b), and pFe ranged from  $0.07 \text{ nmol L}^{-1}$  at the surface to  $0.81$   
20  $\text{nmol L}^{-1}$  at 1500 m (Andrew Bowie, unpublished data); thus much lower than our KEOPS-2  
21 observations at the E site (noting different sampling and digestion methods for pFe were used  
22 for the two cruises).

23

## 24 **3.2 Construction of iron budgets**

25 The primary aim of this work was to use our observations of Fe pools and fluxes to  
26 understand the sources, sinks and biological Fe cycling, and evaluate if Fe supply could meet  
27 demand in both the high-Fe and low-Fe environments in the vicinity of the Kerguelen  
28 archipelago during the KEOPS-2 study. Iron budgets have been constructed for previous  
29 studies in waters fertilized with Fe both naturally (Sarhou et al., 2008; Bowie et al., 2009;  
30 Chever et al., 2010; Ellwood et al., 2014) and artificially (Bowie et al., 2001) as well as low-  
31 Fe conditions (Price and Morel, 1998; Boyd et al., 2005). These budgets have combined



1 geochemical and chemical components to demonstrate that the dominant long-term fluxes of  
2 Fe are associated with the particulate pool (dust supply and particle export), whilst studies on  
3 Fe uptake and microbial cycling have shown that short-term fluxes within the ‘ferrous wheel’  
4 are dominated by biological uptake and remineralisation (Strzepek et al., 2005). Here, we  
5 follow a similar approach to that used by Bowie et al. (2009) for the SAZ-Sense study south  
6 of Tasmania (Australia) at our three study sites. Since all parameters in our iron budget  
7 calculations were only measured at stations R-2, A3-2 and E-5, discussion will focus on these  
8 stations. Data for stations A3-1, E-1 and E-3 are given to provide a context for spatial and  
9 temporal changes in the Fe pools and fluxes during KEOPS-2, and are collated in Table 1.

### 10 **3.2.1 Iron pools**

11 Iron and carbon pools were calculated by integrating the dissolved and particulate profiles  
12 down to the base of the surface mixed layer, defined as the depth where the potential density  
13 equalled the potential density at 10 m + 0.02 kg m<sup>-3</sup> (Park et al., 2014a). The mixed layer  
14 varied from 165 m at station A3-1 to 32 m at station E-3, consistent with the seasonal  
15 shoaling as surface waters warmed, but remained deep (>120 m) on the plateau throughout  
16 the study due to deep mixing as a result of several passing storms.

17 Integrated pools of both dissolved (~5x) and particulate (~10x) Fe were significantly greater  
18 on the plateau (station A3) compared to the plume (station E), with stocks at the reference  
19 station R-2 lower still. Horizontal dFe supply from the plateau to the plume was either or both  
20 via: (i) a geostrophic path looping along the northern side of the PF and then back into the  
21 recirculation feature (d’Ovidio et al., 2015), or (ii) direct Ekman flux transport of Fe-rich  
22 coastal water across the polar front driven by westerly winds, as indicated by radium (Ra)  
23 tracers (Sanial et al., 2015). The latter process is supported by Lagrangian trajectories of water  
24 parcels derived from altimetry, which showed the polar front was not a strong barrier to water  
25 mass movement, with transport of waters across the front taking place on timescale of days-  
26 weeks but being highly variable in space and time (d’Ovidio et al., 2015). The pFe pool  
27 showed the same variability as the dissolved pool at our three study sites and exceeded the  
28 dFe stocks at all sites by factors of approximately 19-26 (A3), 31 (E) and 6 (R-2), although it  
29 is estimated that only ~2-3 % of the particulate pool can be converted into bioavailable forms  
30 by physically or biologically-mediated dissolution (Schroth et al., 2009). If we assume that  
31 station A3-1 represented pre-bloom conditions and the integrated mixed layer pool of 54  
32  $\mu\text{mol dFe m}^{-2}$  was a good estimate of the winter stock, observations show that only 4 weeks

1 later at station A3-2, almost 60 % of the winter stock had been drawn down to  $21 \mu\text{mol m}^{-2}$ . If  
2 annual variability is low, which may not always be the case (Grenier et al., 2015), by late  
3 summer >90% of the winter stock had been used with only  $4.7 \mu\text{mol dFe m}^{-2}$  remaining in the  
4 surface mixed layer at A3 (KEOPS-1 data; Blain et al., 2007). We note this drawdown is  
5 probably a conservative estimate since the winter dFe stock was probably an underestimation  
6 (as evidenced by lower dFe in the mixed layer compared to deep waters at A3-1; Qu  rou   et  
7 al., 2015). Biogenic iron (defined as the Fe associated with living phytoplankton and  
8 phytoplankton biodetritus) was calculated by assuming that all particulate phosphorus (P) was  
9 of biogenic origin, and multiplying the mean particulate P concentration in the mixed layer at  
10 each station by a maximum intracellular Fe/P ratio of  $1.9 \text{ mmol mol}^{-1}$  for natural  
11 phytoplankton assemblages measured by Twining et al. (2004) for Fe-replete conditions.  
12 These calculations follow methods reported in Planquette et al. (2013), and assume particulate  
13 P is not (in part) derived from local rock weathering. van der Merwe et al. (2015) have tested  
14 this assumption using Fe/P ratios in Kerguelen Island basalts and the upper continental crust,  
15 and note that the ~1000-fold increase in pP within suspended particles can only be explained  
16 by pP produced in situ within the mixed layer from dissolved  $\text{PO}_4^-$ . Lithogenic Fe was  
17 calculated by assuming that all particulate aluminium (pAl) was of lithogenic origin and by  
18 multiplying the mean pAl concentration in the mixed layer by a lithogenic Fe/Al ratio of  $0.36$   
19  $\text{mol mol}^{-1}$ , which is the mean value based on basaltic rocks from the Crozet region (0.51;  
20 Gunn et al., 1970) and crustal materials (0.2; Wedephol, 1995). A chosen Fe/Al ratio of  $0.36$   
21  $\text{mol mol}^{-1}$  is also very similar to that of 0.33 used extensively in earlier calculations (Taylor  
22 and McLennan, 1985) and reported for the deep Atlantic Ocean (Sherrell and Boyle, 1992).  
23 This approach is dependent not only on the chosen Fe/Al ratio, but also assumes that  
24 processes other than biological assimilation, such as adsorption and scavenging onto organic  
25 particles, photo-reduction, surface precipitation, and chemically and biologically driven  
26 dissolution, are not significant (Measures et al., 2008; Planquette et al., 2011, 2013; Ellwood  
27 et al., 2014). Since biogenic and lithogenic Fe were calculated independently, their sum may  
28 be less than the observed total particulate Fe concentration. This is likely due to plasticity in  
29 the chosen Fe/Al and Fe/P ratios and differential remineralisation rates for Fe, Al and P.  
30 Nevertheless, our estimates of biogenic and lithogenic Fe provide a perspective on the relative  
31 contributions to the total pFe pool.

32 Reference and plume waters contained roughly an equal fraction of biogenic and lithogenic  
33 Fe. The origin of this biogenic Fe pool will be a combination of biological uptake of dFe,

1 physical adsorption onto suspended biological particles, and conversion from the lithogenic  
2 fraction (likely driven by microbes), with these processes operating on different timescales  
3 (Boyd et al., 2005; Frew et al., 2006; Planquette et al., 2011). On the contrary, the plateau  
4 stations contain 19-69 times more lithogenic Fe than biogenic Fe, consistent with the supply  
5 from the nearby sediments of the plateau and Heard Island, as suspected by Zhang et al.  
6 (2008), van Beek et al. (2008) and discussed in Chever et al. (2010). Measurement of other  
7 geochemical ‘fingerprint’ particulate tracers (such as Al, Mn) on the plateau confirmed the  
8 provenance of Fe supplied from the Kerguelen shelf sediments in the particulate phase (van  
9 der Merwe et al., 2015).

### 10 **3.2.2 Internal iron supply**

11 Vertical fluxes were calculated as follows. A vertical diffusivity ( $K_z$ ) at the base of mixed  
12 layer of  $10^{-5} \text{ m}^2 \text{ s}^{-1}$  was used for the plume and reference site, and a  $K_z$  of  $3 \times 10^{-4} \text{ m}^2 \text{ s}^{-1}$  was  
13 used for the plateau site, estimated from the Shih parameterisations (Shih et al., 2005) using  
14 the Thorpe scale method (Park et al., 2014b). These values are comparable to  $K_z$  values  
15 estimated for KEOPS 1 using the Osborn model ( $4 \times 10^{-4} \text{ m}^2 \text{ s}^{-1}$ ; Osborn, 1980) (Park et al.,  
16 2008a). Vertical diffusivity was multiplied by the vertical dFe gradient for each profile, which  
17 was determined using the linear part of the vertical profiles corresponding to the 150-200 m  
18 depth strata in Figures 3a-3f, consistent with calculations for KEOPS-1 (Blain et al., 2007).  
19 Vertical diffusivity of Fe was negligible at reference and plume sites, but significant on the  
20 plateau due to both the higher vertical diffusivity and the steeper Fe gradient between 150 and  
21 200 m.

22 Upwelling was defined as the vertical velocity ( $w_{ek}$ ) multiplied by the dFe concentration at  
23 200 m, which corresponds to the depth of the remnant winter water. The magnitude of vertical  
24 velocity in this region has recently been studied by Rosso et al. (2014) who used the MIT  
25 general circulation model to examine the sensitivity of the vertical velocity to the horizontal  
26 resolution. They found clear differences in  $w_{ek}$  due to the development of near surface sub-  
27 mesoscale frontal structures that only their highest resolution model was able to resolve.  
28 Rosso et al. (2014) reported vertical velocities for individual water parcels in excess of  $100 \text{ m}$   
29  $\text{day}^{-1}$  in the Kerguelen region, with  $w_{ek}$  stronger in the downstream plume. Both the horizontal  
30 and vertical circulations were much weaker over the plateau since it acts as a natural barrier to  
31 the strong ACC fronts coming from the west. Unfortunately, no seasonal cycle was included  
32 in the model forcing. Therefore the temporal root mean square of the vertical velocity

1 reported in Figure 12(b) of Rosso et al. (2014) was used for the plateau and plume sites ( $w_{ek} =$   
2 0.5 and 1 m d<sup>-1</sup>, respectively) and a conservative value of  $w_{ek} = 0.13$  m d<sup>-1</sup> for the open  
3 Southern Ocean (used by de Baar et al. (1995); originally reported in Gordon et al., 1977) was  
4 chosen for our reference station. Although  $w_{ek}$  was lower on the plateau compared to the  
5 plume, the higher dFe concentration at 200 m resulted in comparable estimates of upwelled  
6 Fe (Table 1).

7 Entrainment of Fe by episodic (intra-seasonal) deepening of the mixed layer has rarely been  
8 taken into account in field studies (Frants et al., 2013) due to the absence of data  
9 characterising the short term variability of the mixed layer depth, yet a recent compilation of  
10 observations (Nishioka et al., 2011; Tagliabue et al., 2014) and modelling studies (Mongin et  
11 al., 2008) suggests that entrainment could be a major vertical supply mechanism fuelling  
12 surface biomass (Carranza et al. 2015). We used more than 6000 vertical profiles of salinity  
13 and temperature collected in the KEOPS-2 regions of interest to estimate the seasonality of  
14 the mixed layer depth and its variability (Supplementary Figure 3). We derived the vertical  
15 supply of Fe by entrainment via hypotheses regarding the relation between the size of mixed  
16 layer depth excursions and their frequency (Supplementary Methods). Entrainment data based  
17 on transient deepening of the mixed layer was not available for station R-2; therefore we  
18 calculated this by multiplying the dFe concentration in winter water (which reflects the dFe  
19 concentration of the winter mixed layer) by the winter mixed layer depth (MLD) and assume  
20 this entrainment event happens once per year. ‘Detrainment’ at R-2 was accounted for by  
21 multiplying this new entrainment flux by the summer-to-winter MLD ratio.

22 For the vertical fluxes, in spring on KEOPS-2, entrainment was the dominant vertical Fe flux  
23 term on the plateau, delivering ~70% of the total vertical supply and tripling the total vertical  
24 flux in comparison to budgets that neglect this process. At the plume and reference sites,  
25 entrainment was comparable to the upwelling flux. Vertical diffusion accounted for 4-8% of  
26 the total vertical supply on the plateau. In contrast, the contribution from dFe entrainment was  
27 much reduced in late summer on KEOPS-1 (42 and 8.8 nmol m<sup>-2</sup> d<sup>-1</sup> for plateau and plume,  
28 respectively) due to the deepening and weakening of the ferricline (Figure 4b). The relative  
29 magnitude of the total vertical Fe supply terms at the three study sites was: plateau > plume >  
30 reference (Table 1, row ‘d’).

31 For the lateral fluxes, the horizontal supply at reference station R-2 was assumed to be zero  
32 since HNLC waters upstream and downstream of this station contained similar dFe and pFe

1 concentrations, and as phytoplankton growth and biomass was low at this site, there would be  
2 little biogenic Fe exported below the mixed layer. On plateau Fe supply at station A3 was  
3 taken from the steady-state box model of Chever et al. (2010) which used the horizontal dFe  
4 gradient and current velocities from Park et al. (2008a) to calculate the lateral flux of 180  
5  $\text{nmol m}^{-2} \text{d}^{-1}$  in the 0-150 m depth band above the plateau; noting this model used KEOPS-1  
6 data. Lateral transport into the plume E stations was assumed to originate from Fe-fertilised  
7 plateau waters that were advected offshore (d'Ovidio et al., 2015). This value was estimated  
8 by assuming that horizontal stirring occurs in a Lagrangian framework, and by using  
9 altimetry-derived geostrophic velocities to determine transports across the plateau boundary.  
10 We also used a depth band of 0–150 m, considered as the winter mixed layer in the plume  
11 over the season. These estimates were combined with direct measurements of the dFe content  
12 of three different types of on-plateau stations to calculate the lateral flux over a 3-month  
13 supply period prior to the spring bloom; namely: (i) two coastal stations near to Kerguelen  
14 Island occupied on KEOPS-2 (stations TEW-1 and TEW-2), (ii) one coastal station close to  
15 Heard Island occupied during KEOPS-1 (station C1), and (iii) the central plateau station A3  
16 considered here. This resulted in  $5.4 \times 10^7$  mol Fe per day being injected into a plume size  
17 (defined at a threshold of  $>0.3 \mu\text{g Chl-a L}^{-1}$  and identified from satellite images) of  $2.5 \times 10^{11}$   
18  $\text{m}^2$  over 90 days in spring (full details of the calculations are contained in d'Ovidio et al.,  
19 2015). This equated to a lateral flux into the plume of  $2400 \text{ nmol m}^{-2} \text{d}^{-1}$  in the October-  
20 November period.

21 By combining our in-situ Fe measurements with estimated ages of the water bodies in the  
22 plume, we calculate a first order exponential scavenging removal constant between 0.041 to  
23  $0.058 \text{ d}^{-1}$ , which equated to a residence time of 17 to 24 days, consistent with estimates based  
24 on the Fe inventory and Fe export in free-floating traps (15-79 days; Laurenceau-Cornec et al.  
25 2015). Since the total of the vertical and lateral fluxes in the plume were more than double  
26 those on the plateau, this may imply that the source waters supplying the plume from the  
27 northern Kerguelen Island shelves (which had a uniquely narrow T-S class in surface waters;  
28 Grenier et al., 2015) were richer in Fe than the plateau further south at A3. This is supported  
29 by observations of dFe in the surface ocean at stations TEW-1 and TEW-2 ( $1.2\text{-}1.8 \text{ nmol L}^{-1}$ )  
30 which were close to Hillsborough Bay in waters only 86 m deep (Qu  rou   et al., 2015).

31 Considering only internal processes (diffusion, upwelling, entrainment, lateral transport) in  
32 supplying Fe to the surface mixed layer, the vertical terms dominated at the reference station,

1 vertical terms were 6-fold greater than lateral terms on the plateau, whereas lateral advection  
2 was the dominant term in the plume (4-5-fold greater than the vertical terms). Since the  
3 particulate Fe stocks were abundant in surface waters (above the winter temperature minimum  
4 layer) and significantly higher than the dissolved pools (most notably on the plateau), it is  
5 likely that a fraction of the suspended lithogenic pFe from Heard Island or the Kerguelen  
6 plateau sediments also contributed to the internal dFe supply and fuelled biological responses.  
7 This is discussed in more detail later.

### 8 **3.2.3 External iron supply**

9 Data on atmospheric Fe fluxes through dust deposition and the solubility of Fe in the dust for  
10 all three study sites were taken from the nearby land-based sampling site “Jacky”  
11 (49°18'42.3”S, 70°07'47.6”E; altitude 250 m) on the Kerguelen Islands, as reported in  
12 Heimbürger et al. (2012, 2013a). Mean total Fe fluxes taken over the period 24/11/2008 to  
13 07/09/2010 were  $500 \pm 390 \text{ nmol m}^{-2} \text{ d}^{-1}$  (Heimbürger et al., 2013a), which was comparable  
14 to the Crozet region upstream ( $895 \text{ nmol m}^{-2} \text{ d}^{-1}$ ; Planquette et al., 2007) and the Southern  
15 Ocean sector south of Australia ( $288\text{-}488 \text{ nmol m}^{-2} \text{ d}^{-1}$ ; Bowie et al., 2009), but greater than  
16 that estimated during the KEOPS-1 study by Wagener et al. (2008) ( $14\text{-}46 \text{ nmol m}^{-2} \text{ d}^{-1}$ ). The  
17 remoteness of the Kerguelen region means it receives low quantities of atmospheric material  
18 (Heimbürger et al., 2012; Wagener et al., 2008) the majority of which is crustal in origin, such  
19 as desert dust from South America, South Africa or Australia (Prospero et al., 2002;  
20 Mahowald, 2007; Bhattachan et al., 2012), although local anthropogenic activities, rock  
21 outcrops and exposed soil may also impact dust fluxes.

22 Atmospheric fluxes were dominated by wet deposition (Heimbürger et al., 2012). Heimbürger  
23 et al. (2013b) calculated the mean ‘soluble’ Fe deposition flux (defined as  $<0.2 \mu\text{m}$ ) using a  
24 median solubility of  $82 \pm 18\%$  in rainwater on Kerguelen Islands. These high solubilities were  
25 attributed to remoteness of the sampling location from dust sources resulting in strong cloud  
26 chemical processing during transport. However, the solubility of Fe dissolved in seawater at  
27 higher pH will be much lower (Schroth et al., 2009; Sedwick et al., 2007). Hence a  
28 conservative value of 10% of Fe that is released into seawater was chosen (Baker et al., 2006;  
29 Mackie et al., 2006) for our budgets here, resulting in a soluble Fe atmospheric deposition  
30 flux to the Kerguelen region of  $50 \text{ nmol m}^{-2} \text{ d}^{-1}$  (Table 1, row ‘f’). This value was lower than  
31 the internal vertical supply on the plateau (~20-fold) and plume (~10-fold), insignificant  
32 compared to the lateral supply to the plume, but comparable to the lateral supply on the

1 plateau. Although volcanic ash has not been considered here for atmospheric Fe supply, this  
2 term may have played an important role for primary productivity on the Kerguelen plateau  
3 during the middle Miocene climate transition (Abrajevitch et al., 2014).

#### 4 **3.2.4 Iron export**

5 Downward Fe and C fluxes were measured directly in free-floating sediment P-traps at the  
6 plateau (A3-2) and plume (E-1, E-3, E-5) stations, and estimated using the  $^{234}\text{Th}$  fluxes and  
7 Fe/Th ratios at the reference site (R-2) (Planchon et al., 2014). The sinking of pFe was by far  
8 the greatest loss term in our budgets, with  $5746 \text{ nmol m}^{-2} \text{ d}^{-1}$  of total Fe exported from the  
9 mixed layer on the plateau, between  $895$  and  $4579 \text{ nmol m}^{-2} \text{ d}^{-1}$  exported at the plume stations  
10 and  $1302 \text{ nmol m}^{-2} \text{ d}^{-1}$  exported at the reference station. The flux of sinking pFe decreased  
11 from station E-1 to E3 to E-5 concurrent with the seasonal progression of the bloom, and  
12 indicating the mixed layer assemblages were efficiently recycling Fe under strong grazing  
13 pressure (Laurenceau-Cornec et al., 2015). The downward total pFe fluxes were greater than  
14 the sum of the vertical, lateral and atmospheric dFe supply on the plateau, but generally less  
15 in the plume.

16 Aluminium was used as a normaliser to estimate the fraction of lithogenic Fe in the exported  
17 material. The percentage lithogenic fraction of total pFe exported at the E stations remained  
18 much the same at each deployment (34-39 %), whereas the lithogenic fraction was a much  
19 larger component at A3-2 (51 %), reflecting the close proximity to sources of particulate  
20 material rich in Fe. The Fe/Al ratio of exported material was higher at E stations (1.0-1.1) and  
21 on the plateau A3-2 (0.87) compared to the Fe/Al ratio of lithogenically-dominated particles  
22 (0.2; Wedepohl, 1995), confirming a significant amount of exported Fe was biogenic in  
23 origin. Interestingly, the Fe/Al export ratios were similar to those associated with suspended  
24 particles at E stations (0.9-1.2) but lower than the Fe/Al of suspended particles at A3-2 (1.2).  
25 This suggests that the biota associated with the plateau bloom at A3 were capable of  
26 efficiently recycling and retaining biogenic particulate Fe in the mixed layer (through rapid  
27 turnover to prevent aggregation and sinking) relative to lithogenic particulate Fe, which had a  
28 shorter residence time and was preferentially exported to depth. This may be due to greater  
29 ballasting of the lithogenic particles (Ellwood et al., 2014), and is consistent with other export  
30 studies which have shown that biologically-processed particles have longer residence times  
31 than lithogenic particles in the mixed layer (Lamborg et al., 2008a). Since P may be lost from  
32 exported particles much faster than Fe due to bacterial remineralisation and zooplankton

1 consumption (Schneider et al., 2003; Lamborg et al., 2008b), it was not appropriate to apply a  
2 biogenic normaliser to the P-trap data as this may underestimate the biogenic Fe component  
3 of particles captured in the traps.

4 Iron export fluxes were greater during the spring study of KEOPS-2 compared to the late  
5 summer study of KEOPS-1 (Table 2). This difference between the KEOPS studies was also  
6 observed in Fe uptake rates (Fourquez et al., 2015). Such observations may be simply related  
7 to the seasonal supply; in other words, greater Fe supply in spring resulted in greater Fe  
8 uptake and export. Determined pFe sinking fluxes were also greater than the CROZEX study  
9 (Planquette et al., 2011), the SAZ-Sense expedition south of Tasmania (Bowie et al., 2009)  
10 and those observed during the FeCycle-I expedition east of New Zealand (Frew et al., 2006),  
11 of similar magnitude to those reported by Bowie et al. (2001) during the SOIREE iron  
12 fertilisation experiment ( $5.2 \mu\text{mol m}^{-2} \text{d}^{-1}$ ), but much lower than Ellwood et al. (2014)  
13 reported for FeCycle-II.

14 The export of particulate organic carbon (POC) into our P-traps followed the same trend to  
15 that of pFe at the E stations, decreasing from  $7.0 \pm 2.3 \text{ mmol m}^{-2} \text{d}^{-1}$  at E-1 to  $2.0 \pm 1.0 \text{ mmol m}^{-2}$   
16  $\text{d}^{-1}$  at E-5 (Table 1). Despite the higher pFe vertical fluxes at A3-2, POC export was lower  
17 than the E stations. The C export fluxes at 200 m at A3-2 using our P-traps (Laurenceau-  
18 Cornec et al., 2015) were similar to results estimated from  $^{234}\text{Th}$  deficits by Planchon et al  
19 (2014;  $2.3 \pm 0.7$  and  $3.8 \pm 0.8 \text{ mmol C m}^{-2} \text{d}^{-1}$ , respectively). Comparison of these POC fluxes  
20 to results (for the A3 plateau site only) obtained during KEOPS-1 illustrates highly dynamic  
21 variations, reflecting the rapid decline of biomass during autumn (Blain et al., 2007).  
22 Specifically, P-trap measurements of POC fluxes at 200 m during KEOPS-1 decreased from  
23  $3.7 \pm 0.3$  to  $1.3 \pm 0.3 \text{ mmol C m}^{-2} \text{d}^{-1}$  over two visits to A3 in February 2005 (Trull et al., 2008),  
24 whereas estimates based on  $^{234}\text{Th}$  at this time, reflecting the previous  $\sim 30$  days of export,  
25 suggested much higher values ( $25 \pm 7 \text{ mmol C m}^{-2} \text{d}^{-1}$ ; Savoye et al. 2008). These variations  
26 illustrate the difficulty of constraining budgets in temporally evolving systems, providing a  
27 cautionary note to our efforts. Additional discussion of temporal and spatial export flux  
28 variations during KEOPS-2 is provided in Laurenceau-Cornec et al. (2015) and Planchon et  
29 al. (2014).



### 1 **3.2.5 Biological iron recycling**

2 Intracellular Fe uptake by phytoplankton and bacteria  $>0.2 \mu\text{m}$  (Fourquez et al., 2015) was  
3 measured at stations A3-2 and E-5 when the bloom was rapidly growing (Cavagna et al.,  
4 2014). Iron uptake fluxes were similar on both the plateau (A3-2) and in the plume (E-5),  
5 ranging between 1120 and 1745  $\text{nmol m}^{-2} \text{d}^{-1}$ . If we assume that the Fe uptake rate of 28.1  
6  $\text{pmol L}^{-1} \text{d}^{-1}$  measured at E-5 (Fourquez et al., 2015) was conservative at E stations, 0.17  $\text{nmol}$   
7  $\text{L}^{-1}$  of Fe could have been consumed in surface waters between the occupations of stations E-  
8 4E and E-5. This is consistent with the observed decrease in surface dFe concentrations from  
9 0.19 to 0.06  $\text{nmol L}^{-1}$  at E-4E and E-5, respectively (Fabien Qu  rou  , pers. comm.). The net  
10 and gross demand calculated at A3 during KEOPS-1 (204 and 408  $\text{nmol m}^{-2} \text{d}^{-1}$ , respectively;  
11 Sarthou et al., 2008) is approximately 3-5 times smaller than the intracellular Fe uptake at A3-  
12 2 during KEOPS-2 for a similar C biomass (mean value of 12.7 and 10.3  $\mu\text{mol L}^{-1}$  POC in  
13 surface at KEOPS-1 and KEOPS-2, respectively; Cavagna et al., 2014), perhaps indicating  
14 luxury uptake as well as important differences in community composition and activity  
15 (primary production). These studies enable opportunity to compare KEOPS-2 to KEOPS-1  
16 data and generate a general picture of the seasonal progress from early spring to late summer,  
17 assuming that inter-annual and spatial variability is low, which may not be the case (Grenier  
18 et al., 2015).

19 The bacterial and mesozooplankton contributions to Fe regeneration were calculated  
20 separately (Table 3). Volumetric values varied between 0.06 and 0.59  $\text{pmol Fe L}^{-1} \text{d}^{-1}$ , and  
21 between 0.02 and 0.08  $\text{pmol Fe L}^{-1} \text{d}^{-1}$ , for bacterial and mesozooplankton Fe regeneration,  
22 respectively. The mesozooplankton rates were much lower than for KEOPS-1 because there  
23 were much fewer individuals (0.26-0.56 per L, compared to about 1-6 individuals per L for  
24 KEOPS-1; see Figure 2 in Carlotti et al., 2008). Total Fe regeneration fluxes ranged from 10  
25 (R-2) to 71 (A3-2)  $\text{nmol m}^{-2} \text{d}^{-1}$ .

26 A similar Fe regeneration calculation was also performed based on the C budget by using the  
27 percentage of gross community production (GCP) that is remineralized for KEOPS-2 and  
28 results from Fe uptake experiments described above. This yielded higher Fe regeneration  
29 estimates in the range 1-11  $\text{pmol L}^{-1} \text{d}^{-1}$ . Specifically, for station A3-2, 23 % of GCP was  
30 remineralised and therefore the Fe regeneration flux in the mixed layer was 1119  $\text{nmol m}^{-2} \text{d}^{-1}$   
31 <sup>1</sup>. Similarly, for station E-5, 34 % of GCP was remineralised resulting in a Fe regeneration  
32 flux of 504  $\text{nmol m}^{-2} \text{d}^{-1}$ . Since the Fe regeneration fluxes based on the C budget are much

1 greater (~16 times) than those calculated using the first approach, this suggests that the  
2 remineralisation efficiency for Fe regeneration appears to be less than that of C.

3 Iron regeneration fluxes can be compared with those from the KEOPS-1 study using the same  
4 first approach above. For station A3 on KEOPS-1, this resulted in a Fe regeneration flux of 1  
5  $\text{pmol L}^{-1} \text{d}^{-1}$  in surface waters. Malits et al. (2014) also calculated the release of bacterial  
6 bound Fe by viral lysis ( $0.42 \text{ pmol L}^{-1} \text{d}^{-1}$ ), which was the dominant loss term during KEOPS-  
7 1 (Brussaard et al., 2008). This value compared to  $1.5 \text{ pmol L}^{-1} \text{d}^{-1}$  determined in zooplankton  
8 grazing experiments (Sarhou et al., 2008), suggesting that grazing and microbial Fe cycling  
9 were in a similar range, and the total Fe regeneration was between 2-3  $\text{pmol L}^{-1} \text{d}^{-1}$  for  
10 KEOPS-1.

11 Importantly, Fe regeneration was much lower during the early compared to late bloom stage  
12 and was dominated by bacterial regeneration in spring (60-90% of total Fe regeneration).  
13 Strezepek et al (2005) estimated Fe regeneration rates (during FeCycle-II) for herbivores  
14 ( $16.5\text{-}18.4 \text{ pmol L}^{-1} \text{d}^{-1}$ ), bacterivores ( $15\text{-}25.5 \text{ pmol L}^{-1} \text{d}^{-1}$ ) and viruses ( $0.4\text{-}28 \text{ pmol L}^{-1} \text{d}^{-1}$ ),  
15 which is equivalent to a total Fe regeneration rate of  $1435\text{-}3236 \text{ nmol m}^{-2} \text{d}^{-1}$  for a 45 m mixed  
16 layer. Bowie et al. (2009) estimated Fe regeneration to be  $261\text{-}1206 \text{ nmol m}^{-2} \text{d}^{-1}$  for the SAZ-  
17 Sense study. So our determined KEOPS-2 mixed layer Fe regeneration rates (71 and 31  $\text{nmol}$   
18  $\text{m}^{-2} \text{d}^{-1}$  at A3-2 and E-5, respectively) were on the lower end of the range reported in other  
19 sectors of the Southern Ocean, and clearly insufficient to meet demand (measured as Fe  
20 uptake) at all stations, indicating a reliance on 'new' Fe supply. This is discussed in more  
21 detail below.

22

### 23 **3.3 Sequestration efficiencies: iron-to-carbon ratios**

24 The mixed layer phytoplankton intracellular Fe/C uptake ratios were calculated directly from  
25 deckboard incubations for stations A3-2 ( $0.007 \text{ mmol mol}^{-1}$ ) and E-5 ( $0.021 \text{ mmol mol}^{-1}$ )  
26 (Table 1). These values are similar to those reported for other natural and artificial iron  
27 fertilisation studies in the Southern Ocean, including for Fe-limited conditions during SOFeX  
28 ( $0.01 \text{ mmol mol}^{-1}$ ; Twining et al., 2004), those inside the KEOPS-1 plateau bloom ( $0.005$   
29  $\text{mmol Fe mol C}^{-1}$ ; Sarhou et al., 2008), but lower than those reported for SAZ-Sense ( $0.06\text{-}$   
30  $0.07 \text{ mmol mol}^{-1}$ ; Bowie et al., 2009).

1 Suspended mixed layer Fe/C ratios (Table 1) were significantly higher than phytoplankton  
2 intracellular uptake ratios. This finding is likely the result of the contribution of lithogenic and  
3 detrital Fe to suspended material Fe/C ratios, and is consistent with the removal of C at a  
4 faster rate than that of Fe, and for Fe to be added through new sources after phytoplankton  
5 uptake. Differences may also arise because of luxury uptake, the timescale of integration in  
6 deckboard experiments compared to Fe/C ratios in ocean suspended and sinking particles  
7 (which are broadly similar – see below), and/or that our system was not in steady-state. Also,  
8 since a Ti-citrate-EDTA wash was used to remove extracellular surface Fe during the  
9 incubation experiments, but not on particles collected in the ISPs and P-traps, our suspended  
10 and sinking pFe concentrations include Fe present within cells, adsorbed to cell walls, detrital  
11 Fe and lithogenic Fe. This would tend to increase Fe/C in suspended particles. Differences  
12 between intracellular and suspended mixed layer Fe/C ratios may also derive from the C term,  
13 since the ISP sampling includes detrital material as well as living cells. We also note that  
14 suspended pFe data is the sum of 1-53um and >53um size fractions collected by ISPs and thus  
15 may also include some sinking particles. This may affect the suspended Fe/C ratios.

16 In addition to the ratio of “total“ particulate (biogenic+lithogenic) Fe over POC (Fe/C) in  
17 suspended particles discussed above, we also calculated the ratio of biogenic Fe over POC  
18 (i.e.,  $Fe_{bio}/C$ ) following methods discussed in section 3.2.1. Profiles are shown in Figure 5.

19 Suspended Fe/C ratios were remarkably similar at all E stations and station R-2, but higher on  
20 the plateau at A3 stations (Table 1). We also observed generally surface-to-deep increases in  
21 Fe/C ratios in suspended particles at all stations (Figure 5), consistent with earlier findings  
22 (Frew et al. 2006). The vertical profiles of  $Fe_{bio}/C$  showed similar structure at the three study  
23 sites, with a general decreasing trend from the surface to sea floor (opposite to that of Fe/C),  
24 noting that a constant Fe/P was used to estimate the  $Fe_{bio}$  component. These findings indicate  
25 that Fe is preferentially retained within, and adsorbed to, sinking particles (i.e., scavenging  
26 drives the “total” Fe/C ratio), but biogenic Fe is recycled at a faster rate compared to C,  
27 similar to macronutrients N and P. A preferential loss of C relative to Fe from sinking  
28 material implies that an external input of Fe is required to sustain a downward flux of carbon.

29 At station R-2, the Fe/C ratio peaked at 500 m, most likely due to lithogenic particulate Fe  
30 input (and not C) from the Leclaire Rise (see above) (note this peak was not seen in the  
31  $Fe_{bio}/C$  ratios). At E stations, the Fe/C ratio showed maximum values in mesopelagic  
32 intermediate waters in the 600-1000 m depth range. We also believe this was due to the lateral

1 transport of lithogenic particulate Fe (and not C) from the plateau (seafloor at ~600 m) into  
2 the plume. This is supported by the absence of this feature in the  $Fe_{bio}/C$  ratios for E stations.  
3  $Fe/C$  ratios in deep waters were much higher at A3 stations (26-38  $mmol\ mol^{-1}$ ) compared to  
4 R-2 (4  $mmol\ mol^{-1}$ ) and E stations (5-7  $mmol\ mol^{-1}$ ), indicating enrichment of lithogenic  
5 particulate Fe above the plateau. Some fraction of this lithogenic Fe will be accessible to the  
6 biota and then be incorporated into the biogenic Fe pool. This is confirmed by modification of  
7 the  $Fe/Al$  ratio (van der Merwe et al., 2015). Inclusion of the biologically available fraction of  
8 the lithogenic Fe flux is therefore required to calculate fully the yield of carbon exported per  
9 unit Fe injected, consistent with Planquette et al. (2011) and Pollard et al. (2009).

10 Interestingly, although  $Fe/C$  ratios varied greatly between stations (0.2-37  $mmol\ mol^{-1}$ ), the  
11  $Fe_{bio}/C$  ratio fell within a narrow band (0.01-0.08  $mmol\ mol^{-1}$  for all stations and depths),  
12 which encompasses the elemental ratios of Fe-replete (0.04  $mmol\ mol^{-1}$ ) and Fe-limited (0.01  
13  $mmol\ mol^{-1}$ ) large diatoms (Sunda and Huntsman, 1995; de Baar et al., 2008). This highlights  
14 the tight coupling between  $Fe_{bio}$  and POC in the absence of new sources of Fe, and allow us to  
15 estimate the relative remineralisation efficiencies for Fe versus C. The  $Fe_{bio}/C$  data contrast  
16 with the findings of Planquette et al. (2011) for the CROZEX study who observed variable  
17  $Fe_{bio}/C$  ratios to the north of Crozet (Fe-fertilised region) which were on average much higher  
18 than those found to the south (Fe-limited region). The fraction of  $Fe_{bio}$  relative to lithogenic  
19 Fe in particles collected below the mixed layer also depends on the stage of the bloom, the  
20 nature and magnitude of supply of new lithogenic particles, and the rate of conversion from  
21 lithogenic-to-biogenic Fe (Lam et al., 2006; Frew et al., 2006; Lam and Bishop, 2008). These  
22 factors are highly variable in the Kerguelen region and this explains the wide range of  $Fe_{bio}$ -  
23 to-“total” Fe values in particles observed during KEOPS-2.

24 The  $Fe/C$  export ratio of sinking particles in our traps were similar to suspended mixed layer  
25 ratios for the E stations, but slightly higher at A3-2 (Figure 5), possibly due to the sinking of  
26 recently supplied lithogenics over the plateau. Both pFe and POC export fluxes decreased  
27 during bloom development at E stations, indicating the mixed layer became more retentive for  
28 both Fe and C. This is consistent with the picture that emerges from the E time series from  
29 primary and export production estimates which show that production was moderate and  
30 matched by the moderate export during our visits (Planchon et al., 2014; Trull et al., 2015;  
31 Cavagna et al., 2014).

1 Since POC export fluxes during spring (KEOPS-2) were similar to late summer (KEOPS-1),  
2 but pFe export fluxes were higher in spring compared to summer (Table 2), this resulted in a  
3 generally higher carbon sequestration efficiency (lower Fe/C) during late summer, consistent  
4 with a rapidly exporting ecosystem during bloom decline. The exported particles may have  
5 been dominated by more lithogenics and much more processed in KEOPS-2 compared to  
6 KEOPS-1, where the system had already ran out of Fe. It was also expected that growing  
7 communities during KEOPS-2 would retain dFe through luxury uptake, which may also result  
8 in observed generally higher Fe/C ratios in sinking particles during the spring bloom  
9 (KEOPS-2, FeCycle-II) compared to austral summer conditions (KEOPS-1, CROZEX,  
10 FeCycle-I; Blue Water Zone; Morris and Charette, 2013) (Table 2 and Figure 6).

11 Morris and Charette (2013) presented a detailed synthesis of  $^{234}\text{Th}$ -derived POC export and  
12 dFe budgets in studies where natural iron fertilisation fuels the substantial phytoplankton  
13 blooms observed in the Southern Ocean. Where data is available to calculate the seasonal  
14 Fe/C ratios, an order of magnitude variation (0.006-0.06) is observed between different  
15 Southern Ocean regions. It is likely that Fe/C ratio variations (Table 2) reflect both  
16 experimental methodologies, different calculation approaches, observational limitations and  
17 system complexities. Le Moigne et al. (2014) have also recently shown that variability in the  
18 carbon sequestration efficiency is related to the mode of Fe delivery.

19

### 20 **3.4 Iron supply versus demand**

21 Using calculated flux estimates, a comparison of Fe supply and demand at the three sites  
22 around the Kerguelen archipelago in spring was possible (Figure 7). In our short-term iron  
23 biogeochemical budgets, the total dFe supply from ‘new’ sources (calculated as the sum of  
24 diffusion, upwelling, vertical and lateral advection, and atmospheric dust) to surface waters of  
25 the plume was more than twice that above the plateau and >20 times greater than at the  
26 reference station (Table 1). The Fe demand (measured by cellular Fe uptake) in the plume was  
27 similar (1.5 times greater) to the plateau but >40 times greater than at the reference station.  
28 ‘New’ Fe supply was 14-94 times greater than ‘recycled’ Fe supply (‘iron remineralisation’;  
29 row ‘i’ in Table 1) from bacterial regeneration and zooplankton grazing. This contrasts with  
30 the findings of Bowie et al. (2009) for SAZ-Sense who reported recycled fluxes that were

1 broadly comparable with new Fe supply in the SAZ in summer at study sites further from  
2 natural iron fertilisation.

3 Since Fe supply from 'new' sources was greater than the Fe demand (uptake minus  
4 remineralisation as a 'recycled' Fe source) at all stations (R-2, A3-2 and E-5), this resulted in  
5 a positive value for row 'k' in Table 1 (i.e., there was no additional Fe required to balance the  
6 dissolved budget). This finding is consistent with other observations at both the plateau and  
7 plume sites which were Fe replete in early spring, but somewhat surprising for the HNLC  
8 reference site R-2. This may partly be a result of an over-estimate of the atmospheric supply  
9 used in calculations presented here from literature data. Another explanation is that the  
10 parameters used in our 'short-term' iron budget calculations are decoupled in time (e.g., there  
11 will be an offset between the mechanisms for organism acquisition of Fe and the processes  
12 resulting in Fe-laden particles leaving the upper ocean), and the short-term Fe budget is based  
13 on an 'instantaneous picture' of different fluxes that were not in steady-state.

14 Interestingly, at station A3-2, the sink processes (Fe export and uptake) are so large and the  
15 regenerated Fe flux so small, that the total (dissolved + particulate) Fe losses are far greater  
16 than the net dFe supply (Figure 7a). In other words, to a first order the budget is not balanced  
17 with known sources of Fe insufficient to account for the downward flux, even if we only  
18 accounted for the non-lithogenic particulate Fe export flux (row 'l' in Table 1). Assuming all  
19 flux calculations to be correct within the estimated error bounds in Table 1, this implies there  
20 is a missing flux term in the budget at A3 and this is likely lithogenic pFe from the Kerguelen  
21 plateau and/or Heard Island (and this may be converted to biogenic Fe). Currently, we do not  
22 invoke a lithogenic pFe to dFe transfer in the budget, which could increase the Fe supply on  
23 the plateau significantly, although at present we do not know what fraction of particulate  
24 material is converted into the dissolved form. This will vary largely with the mineralogy  
25 (Schroth et al., 2009), provenance of the particles, and seawater characteristics (e.g., organic  
26 complexation; Shaked and Lis, 2012). Indeed, Thuróczy et al. (2012) previously measured  
27 organic complexation in Antarctic waters and discussed the role of ligands in transporting and  
28 dissolving pFe into dFe, using theoretical data provided by Borer et al. (2005).

29 By applying a solubility of 2.5 % used for KEOPS-1 at A3 to enable Fe supply to meet  
30 demand (Blain et al., 2007), this would provide an extra  $10\text{-}34 \mu\text{mol m}^{-2}$  of dFe to the mixed  
31 layer over the plateau in KEOPS-2, approximately doubling the dFe standing stock. These  
32 values are comparable to our observations and suggest that particulate material plays a major

1 role in the supply of dFe (van der Merwe et al., 2015). Further, if we assume pFe from glacial  
2 melt is delivered over a 3 month period, this would provide an additional  $111\text{-}387\text{ nmol m}^{-2}\text{ d}^{-1}$   
3 <sup>1</sup> to the mixed layer at A3, values of similar magnitude to the individual vertical and lateral  
4 supply terms. Whilst a dissolution estimate of 2.5 % may be considered to be at the upper  
5 extent of the range, Schroth et al. (2009) have reported that 2-3 % of Fe is soluble in glacial  
6 flour which can remain suspended in surface water for several months after delivery from  
7 Kerguelen or Heard Islands.

8 The release of Fe to biota via conversion of lithogenic to biogenic Fe has been previously  
9 suggested (Lam et al., 2006; Frew et al., 2006; Borer et al., 2009; Planquette et al., 2011) and  
10 the present work strongly supports this hypothesis, with our data (Figure 5) indicating that  
11 biogenic Fe has a longer residence time in the upper ocean than lithogenic Fe which is not  
12 accessed by biota. The role of pFe in supplying bioavailable Fe is also supported by the  
13 similarity of the pFe and dFe profile shapes in Figure 3, which infer that pFe may be  
14 contributing to the control of dFe, either by supplying it or because biogenic particles are  
15 controlling both.

16 Finally, our estimation of Fe supply and regeneration allowed us to estimate an *fe* ratio,  
17 defined by Boyd et al. (2005) as  $fe = \text{uptake of new} / \text{uptake of new} + \text{regenerated Fe}$ . For the  
18 plume region, *fe* was 1.4 (Table 1). This was higher than the *fe* ratio calculated for KEOPS-1  
19 (0.49; Sarthou et al. 2008), which at that time was comparable to the average *f*-ratio for  
20 nitrogen of 0.41 (corresponding to  $\text{NO}_3^-$  uptake / ( $\text{NO}_3^-$  uptake +  $\text{NH}_4^+$  uptake); Mosseri et al.,  
21 2008), indicating that both  $\text{NH}_4^+$  and regenerated Fe could support export production.  
22 Conversely, the KEOPS-2 *f*-ratio was higher (up to 0.9; Cavagna et al., 2014), indicating that  
23 primary production was mainly sustained by nitrate uptake. The *fe* ratios for both KEOPS  
24 studies were much higher than the *fe* ratio estimated during FeCycle-I (0.17, Boyd et al.,  
25 2005) and SAZ-Sense (0.06-0.16; Bowie et al., 2009). This confirms that in the Kerguelen  
26 region, there are sufficient ‘new’ sources of Fe delivered on a seasonal timescale  
27 (predominantly via intra-seasonal entrainment, winter mixing, lateral transport and particulate  
28 Fe dissolution) available to sustain the massive bloom observed in spring.

29

#### 30 **4 Conclusions**

31 The complex regional circulation, multiple iron sources, and transport pathways above and  
32 downstream of the naturally fertilised Kerguelen plateau region results in a mosaic of

1 phytoplankton blooms. The budgets presented here result from direct measurements of the Fe  
2 inventories and fluxes between different pools. The system was not in steady-state during the  
3 period of the KEOPS-2 observations, and the exchange of Fe between the dissolved, biogenic  
4 and lithogenic pools was highly dynamic in time and space. Our analysis highlights the  
5 important role of pFe, the inherent heterogeneity and biogeochemical differences associated  
6 with particulates within and exported below the mixed layer, and the lithogenic to biogenic  
7 conversion pathways.

8 This study also highlights the significance not only of the mode of Fe fertilisation on the  
9 plateau (predominantly vertical) versus the plume (predominantly lateral), but also of the  
10 relative magnitude. Importantly, since the Fe supply from ‘new’ sources to the plume was  
11 more than double that above the plateau, this implies the waters that supply the plume are not  
12 the same as those at station A3 on the southern plateau, and the plume must be supplied with  
13 water from the northern part of the plateau or Kerguelen coastal waters which are richer in  
14 dFe (Qu  rou   et al., 2015; Trull et al., 2015). This source of Fe, which will contain a large  
15 fraction of particulate material (van der Merwe et al., 2015) that is transported off the  
16 Kerguelen plateau, is therefore an important but previously unquantified contribution to the  
17 downward flux of Fe exiting the upper ocean in the plume. Moreover, the KEOPS-2 results  
18 are tightly linked to the mode of Fe supply that is different from dust deposition or purposeful  
19 additions, and to the concomitant supply of major nutrients, and this has consequences for the  
20 carbon sequestration efficiency of the system. When Fe supply is predominantly vertical (as it  
21 is at station A3), then the C sequestration efficiency is lower (i.e., higher Fe/C) as C would be  
22 re-supplied to the mixed layer as well as Fe. This coupling has important implications for  
23 geoengineering schemes that propose to increase the supply of Fe to surface waters by  
24 pumping waters from below.

25 Future efforts should focus on the quantification of the full seasonal cycle of Fe delivery,  
26 which will be fundamental to closing the iron budget around the Kerguelen archipelago over  
27 annual timescales. This will allow assessment of the important longer-term climatic and  
28 ecosystem implications with changes in the nature and strength of Fe supply with physical  
29 (weakening overturning circulation, warming, increased stratification), and chemical (ocean  
30 acidification, deoxygenation) environmental forcings, together with increases in glacial melt,  
31 rainfall and dust deposition on a warming planet.

32



## 1 **Author contributions**

2 A. R. B. designed the iron budgets, performed the calculations and prepared the manuscript  
3 with contributions from all co-authors. P. vd M., F. Q., G. S., F. C. and A. T. collaborated on  
4 trace metal sampling, analyses and interpretation, M. F. and I. O. were responsible for  
5 biological cycling, T. T. for carbon dynamics and the P-trap deployments, F. P. for Th-based  
6 export, and J.-B. S. for vertical flux estimates. S. B. designed the overall KEOPS-2 study and  
7 helped with budget calculations.

8

## 9 **Acknowledgements**

10 We thank the captain B. Lassiette, officers and crew of M.D. *Marion Dufresne*, Pierre  
11 Sangiardi (Institut Paul Emile Victor) and the Institut National des Sciences de l'Univers for  
12 voyage logistics and their support of the science, and voyage leader Bernard Quéguiner  
13 (Institut Méditerranéen d'Océanologie) and chief scientist Stéphane Blain (LOMIC,  
14 Université Pierre et Marie) for leading the KEOPS-2 expedition. We acknowledge Thomas  
15 Rodemann (UTAS) for CHN analysis in the Central Science Laboratory, together with  
16 members of the ISP and P-trap teams for support at sea. Michael Ellwood (Australian  
17 National University) kindly loaned the TMR for the project. Access to ICP-MS was provided  
18 through Australian Research Council LIEF funds (LE0989539). The altimeter and  
19 colour/temperature products for the Kerguelen area were produced by Ssalto/Duacs and CLS  
20 with support from CNES, and kindly prepared by Emmanuel Laurenceau-Cornec (UTAS) and  
21 Francesco d'Ovidio (LOCEAN – IPSL, Université Pierre et Marie Curie). We thank Isabella  
22 Rosso (Australian National University) for useful discussion.

23 This KEOPS-2 project was supported by the French Research program of INSU-CNRS  
24 LEFE–CYBER ('Les enveloppes fluides et l'environnement' – 'Cycles biogéochimiques,  
25 environnement et ressources'), the French ANR ('Agence Nationale de la Recherche', SIMI-6  
26 program, ANR-2010-BLAN-614 KEOPS2 and, ANR-10-JCJC-606 ICOP), the French CNES  
27 program ('Centre National d'Etudes Spatiales') and the French Polar Institute IPEV (Institut  
28 Polaire Paul–Emile Victor). The Australian participation in the project was supported by the  
29 Antarctic Climate and Ecosystems Cooperative Research Centre and a University of  
30 Tasmania 'Rising Stars' award to the lead author.

1 We thank two anonymous reviewers for their very constructive comments which improved  
2 our manuscript.  
3

## 1 **References**

- 2 Abrajvitch, A., Roberts, A. P., and Kodama, K.: Volcanic iron fertilization of primary  
3 productivity at Kerguelen Plateau, Southern Ocean, through the Middle Miocene Climate  
4 Transition, *Palaeogeogr. Palaeoclimatol. Palaeoecol.*, 410, 1–13,  
5 doi:10.1016/j.palaeo.2014.05.028, 2014.
- 6 Assmy, P., et al.: Thick-shelled, grazer-protected diatoms decouple ocean carbon and silicon  
7 cycles in the iron-limited Antarctic Circumpolar Current, *Proc. Natl. Acad. Sci. USA* 110,  
8 20633–20638, doi:10.1073/pnas.1309345110, 2013.
- 9 Baker, A. R., Jickells, T. D., Witt, M., and Linge, K. L.: Trends in the solubility of iron,  
10 aluminium, manganese and phosphorus in aerosol collected over the Atlantic Ocean, *Mar.*  
11 *Chem.*, 98(1), 43–58, doi:10.1016/j.marchem.2005.06.004, 2006.
- 12 Bhattachan, A., D’Odorico, P., Baddock, M. C., Zobeck, T. M., Okin, G. S., and Cassar, N.:  
13 The Southern Kalahari: A potential new dust source in the Southern Hemisphere?, *Environ.*  
14 *Res. Lett.*, 7, 1–7, doi:10.1088/1748-9326/7/2/024001, 2012.
- 15 Bishop, J. K. B., Lam, P. J., and Wood T. J.: Getting good particles: Accurate sampling of  
16 particles by large volume in-situ filtration, *Limnol. Oceanogr.: Methods*, 10, 681-710,  
17 doi:10.4319/lom.2012.10.681, 2012.
- 18 Blain S. et al.: Effect of natural iron fertilization on carbon sequestration in the Southern  
19 Ocean, *Nature*, 446, 1070-1074, doi:10.1038/nature05700, 2007.
- 20 Blain, S., Quéguiner, B., and Trull, T.: The natural iron fertilization experiment KEOPS  
21 (Kerguelen Ocean and Plateau compared Study): An overview, *Deep Sea Res. II* 55, 559-565,  
22 doi:10.1016/j.dsr2.2008.01.002, 2008a.
- 23 Blain, S., Sarthou, G., and Laan, P.: Distribution of dissolved iron during the natural iron-  
24 fertilization experiment KEOPS (Kerguelen Plateau, Southern Ocean), *Deep Sea Res. II* 55,  
25 594-605, doi: 10.1016/j.dsr2.2007.12.028, 2008b.
- 26 Blain, S., Capparos, J., Guéneuguès, A., Obernosterer, I., and Oriol, L.: Distributions and  
27 stoichiometry of dissolved nitrogen and phosphorus in the iron-fertilized region near  
28 Kerguelen (Southern Ocean), *Biogeosciences*, 12, 623-635, doi:10.5194/bg-12-623-2015,  
29 2015.
- Borer, P. M., Sulzberger, B., Reichard, P., and Kraemer, S. M.: Effect of siderophores

1 on the light-induced dissolution of colloidal iron(III)(hydr)oxides, *Mar. Chem.*, 93, 179–193,  
2 doi:10.1016/j.marchem.2004.08.006, 2005.

3 Borer, P., Sulzberger, B., Hug, S. J., Kraemer, S. M., and Kretzschmar, R.: Photoreductive  
4 dissolution of iron(III) (hydr)oxides in the absence and presence of organic ligands:  
5 experimental studies and kinetic modelling, *Environ. Sci. Technol.*, 43 (6), 1864–1870,  
6 doi:10.1021/es801352k, 2009.

7 Bowie A. R. and Lohan M. C.: Analysis of Iron in Seawater. Chapter 12 in: “Practical  
8 Guidelines for the Analysis of Seawater”, Wurl O. (Ed.), Taylor and Francis, Boca Raton  
9 (USA), Chapter 12, pp. 235-257, ISBN 978-1-4200-7306-5,  
10 doi:10.1201/9781420073072.ch12, 2009.

11 Bowie A. R., Maldonado M. T., Frew R. D., Croot P. L., Achterberg E. P., Mantoura R. F. C.,  
12 Worsfold P. J., Law C. S., and Boyd P. W.: The fate of added iron during a mesoscale  
13 fertilisation experiment in the Southern Ocean. *Deep Sea Res. II*, 48, 2703-2743, doi:  
14 10.1016/S0967-0645(01)00015-7, 2001.

15 Bowie A. R., Lannuzel D., Remenyi T.A., Wagener T., Lam P.J., Boyd P.W., Guieu C.,  
16 Townsend A.T., and Trull T.W.: Biogeochemical iron budgets of the Southern Ocean south of  
17 Australia: Decoupling of iron and nutrient cycles in the subantarctic zone by the summertime  
18 supply, *Glob. Biogeochem. Cycles*, 23, GB4034, doi:10.1029/2009GB003500, 2009.

19 Bowie A. R., Townsend A. T., Lannuzel D., Remenyi T., van der Merwe P.: Modern  
20 sampling and analytical methods for the determination of trace elements in marine particulate  
21 material using magnetic sector ICP-MS, *Anal. Chim. Acta*, 676 (1-2) 15-27,  
22 doi:10.1016/j.aca.2010.07.037, 2010

23 Boyd, P. W. and Ellwood, M. J.: The biogeochemical cycle of iron in the ocean, *Nat. Geosci.*,  
24 3, 675–682, doi:10.1038/ngeo964, 2010.

25 Boyd P., et al.: A mesoscale phytoplankton bloom in the polar Southern Ocean stimulated by  
26 iron fertilization, *Nature*, 407, 695–702, doi:10.1038/35037500, 2000.

27 Boyd, P.W. et al.: FeCycle: Attempting an iron biogeochemical budget from a mesoscale SF6  
28 tracer experiment in unperturbed low iron waters, *Glob. Biogeochem. Cycles*, 19, GB4S20,  
29 doi:10.1029/2005GB002494, 2005.

1 Boyd, P. W., et al.: Mesoscale Iron Enrichment Experiments 1993-2005: Synthesis and Future  
2 Directions, *Science*, 315, 612-617, doi:10.1126/science.1131669, 2007.

3 Breitbarth, E., et al.: Iron biogeochemistry across marine systems – progress from the past  
4 decade, *Biogeosciences*, 7(3), p. 1075-1097, doi:10.5194/bg-7-1075-2010, 2010.

5 Brussaard, C. P. D., Timmermans, K. R. , Uitz, J., and Veldhuis, M. J. W.: Virioplankton  
6 dynamics and virally induced phytoplankton lysis versus microzooplankton grazing southeast  
7 of the Kerguelen (Southern Ocean), *Deep-Sea Research II* 55, 752–765,  
8 doi:10.1016/j.dsr2.2007.12.034, 2008.

9 Carlotti, F., Thibault-Botha, D., Nowaczyk, A. and Lefèvre, D.: Zooplankton community  
10 structure, biomass and role in carbon fluxes during the second half of a phytoplankton bloom  
11 in the eastern sector of the Kerguelen shelf (January-February 2005), *Deep Sea Res. II*, 55,  
12 720-733, doi: 10.1016/j.dsr2.2007.12.010, 2008.

13 Carlotti, F., Jouandet, M.-P., Nowaczyk, A., Harmelin-Vivien, M., Lefèvre, D., Guillou, G.,  
14 Zhu, Y., and Zhou, M.: Mesozooplankton structure and functioning during the onset of the  
15 Kerguelen phytoplankton bloom during the Keops2 survey, *Biogeosciences Discuss.*, 12,  
16 2381-2427, doi:10.5194/bgd-12-2381-2015, 2015.Carranza, M. M., and Gille, S. T.: Southern  
17 Ocean wind-driven entrainment enhances satellite chlorophyll-a through the summer, *J.*  
18 *Geophys. Res. Oceans*, 120, 304–323, doi:10.1002/2014JC010203, 2015.

19 Cavagna, A. J., Fripiat, F., Elskens, M., Dehairs, F., Mangion, P., Chirurgien, L., Closset, I.,  
20 Lasbleiz, M., Flores–Leiva, L., Cardinal, D., Leblanc, K., Fernandez, C., Lefèvre, D., Oriol,  
21 L., Blain, S., and Quéguiner, B.: Biological productivity regime and associated N cycling in  
22 the vicinity of Kerguelen Island area, Southern Ocean, *Biogeosciences Discuss.*, 11, 18073-  
23 18104, doi:10.5194/bgd-11-18073-2014, 2014.Chever, F., Sarthou, G., Bucciarelli, E., Blain  
24 S., and Bowie A. R.: An iron budget during the natural iron fertilization experiment KEOPS  
25 (Kerguelen Island, Southern Ocean), *Biogeosciences*, 7, 455–468, doi:10.5194/bg-7-455-  
26 2010, 2010.

27 Christaki, U., Lefèvre, D., Georges, C., Colombet, J., Catala, P., Courties, C., Sime-Ngando,  
28 T., Blain, S., and Obernosterer, I.: Microbial food web dynamics during spring phytoplankton  
29 blooms in the naturally iron-fertilized Kerguelen area (Southern Ocean), *Biogeosciences*, 11,  
30 6739-6753, doi:10.5194/bg-11-6739-2014, 2014.Cutter, G. A. and Bruland K. W.: Rapid and

1 noncontaminating sampling system for trace elements in global ocean surveys, *Limnol.*  
2 *Oceanogr: Methods*, 10, 425-436, doi:10.4319/lom.2012.10.425, 2012.

3 de Baar, H. J. W., de Jong, J. T. M., Bakker, D. C. E., Löscher, B. M., Veth, C., Bathmann,  
4 U., and Smetacek, V.: Importance of iron for plankton blooms and carbon dioxide drawdown  
5 in the Southern Ocean, *Nature*, 373, 412-415, doi:10.1038/373412a0, 1995.

6 de Baar, H. J. W. et al.: Synthesis of iron fertilization experiments: From the iron age in the  
7 age of enlightenment, *J. Geophys. Res.*, 110, C09S16, doi:10.1029/2004JC002601, 2005.

8 de Baar, H. J. W. et al.: Efficiency of carbon removal per added iron in ocean iron  
9 fertilization, *Mar. Ecol. Prog. Ser.*, 364, 269-282, doi:10.3354/meps07548, 2008.

10 de Jong J.T.M. et al.: Dissolved iron at sub-nanomolar levels in the Southern Ocean as  
11 determined by ship-board analysis, *Anal. Chim. Acta*, 377, 113-124, doi: 10.1016/S0003-  
12 2670(98)00427-9, 2008.

13 de Jong, J., Schoemann, V., Lannuzel, D., Croot, P., de Baar, H., and Tison, J.-L.: Natural  
14 iron fertilization of the Atlantic sector of the Southern Ocean by continental shelf sources of  
15 the Antarctic Peninsula, *J. Geophys. Res.*, 117, G01029, doi:10.1029/2011JG001679, 2012.

16 d'Ovidio, F., Della Penna, A., Trull, T. W., Nencioli, F., Pujol, I., Rio, M. H., Park, Y.-H.,  
17 Cotté, C., Zhou, M., and Blain, S.: The biogeochemical structuring role of horizontal stirring:  
18 Lagrangian perspectives on iron delivery downstream of the Kerguelen plateau,  
19 *Biogeosciences Discuss.*, 12, 779-814, doi:10.5194/bgd-12-779-2015, 2015.Ellwood, M. J.,  
20 Nodder, S. D., Boyd, P. W., King, A. L., Hutchins, D. A., and Wilhelm, S. W.: Pelagic iron  
21 cycling during the subtropical spring bloom, east of New Zealand, *Mar. Chem.*, 160, 18-33,  
22 doi: 10.1016/j.marchem.2014.01.00, 2014.

23 Fourquez, M., Obernosterer, I., Davies, D. M., Trull, T. W., and Blain, S.: Microbial iron  
24 uptake in the naturally fertilized waters in the vicinity of the Kerguelen Islands:  
25 phytoplankton–bacteria interactions, *Biogeosciences*, 12, 1893-1906, doi:10.5194/bg-12-  
26 1893-2015, 2015.Frants, M. et al.: Analysis of horizontal and vertical processes contributing  
27 to natural iron supply in the mixed layer in southern Drake Passage, *Deep Sea Res. II*, 90, 68–  
28 76, doi:10.1016/j.dsr2.2012.06.001, 2013.

29 Frew, R. D., Hutchins D. A., Nodder S., Sanudo-Wilhelmy S., Tovar-Sanchez A., Leblanc K.,  
30 Hare C. E., and Boyd P. W.: Particulate iron dynamics during FeCycle in subantarctic waters

1 southeast of New Zealand, *Glob. Biogeochem. Cycles*, 20, GB1S93,  
2 doi:10.1029/2005GB002558, 2006.

3 Gerringa, L. J. A., Blain, S., Laan, P., Sarthou, G., Veldhuis, M. J. W., Brussaard, C. P. D.,  
4 Viollier, E., Timmermans, K. R.: Fe-binding dissolved organic ligands near the Kerguelen  
5 Archipelago in the Southern Ocean (Indian sector), *Deep Sea Res. II*, 55, 606-621,  
6 doi:10.1016/j.dsr2.2007.12.007, 2008.

7 Gordon, A. L., Taylor, H. W., and Georgi, D. T.: Antarctic oceanography zonation. In:  
8 Proceedings of SCOR/SCAR Polar Oceans Conference, Montreal, Canada, May 5–11, 1974.  
9 Dunbar, M.J. (Ed.), Arctic Institution of North America. McGill University, Montreal, 1977.

10 Grenier, M., Della Penna, A., and Trull, T. W.: Autonomous profiling float observations of  
11 the high-biomass plume downstream of the Kerguelen Plateau in the Southern Ocean,  
12 *Biogeosciences*, 12, 2707-2735, doi:10.5194/bg-12-2707-2015, 2015. Gunn, B. M., Coyyll,  
13 R., Watkins, N. D., Abranson, C. E., and Nougier, J.: Geochemistry of an oceanite–  
14 ankaramite–basalt suite from East Island, Crozet Archipelago, *Contrib. Mineral. Petrol.*,  
15 28(4), 319–339, doi:10.1007/BF00388954, 1970.

16 Heimburger, A., Losno, R., Triquet, S., Dulac, F., and Mahowald, N.: Direct measurements of  
17 atmospheric iron, cobalt, and aluminum-derived dust deposition at Kerguelen Islands, *Glob.*  
18 *Biogeochem. Cycles*, 26, GB4016, doi:10.1029/2012GB004301, 2012.

19 Heimburger, A., Losno, R., Triquet, S. and Bon Nguyen, E.: Atmospheric deposition fluxes of  
20 26 elements over the Southern Indian Ocean: time series on Kerguelen and Crozet Islands,  
21 *Glob. Biogeochem. Cycles*, 27-2, 440-449, doi:10.1002/gbc.20043, 2013a.

22 Heimburger, A., Losno, R., and Triquet, S.: Solubility of iron and other trace elements over  
23 the Southern Indian Ocean, *Biogeosciences*, 10, 6617-6628, doi:10.5194/bg-10-6617-2013,  
24 2013b.

25 Homoky, W. B., John, S. G., Conway, T. M. and Mills, R. A.: Distinct iron isotopic  
26 signatures and supply from marine sediment dissolution, *Nat. Comm.*, 4, 2143,  
27 doi:10.1038/ncomms3143, 2013.

28 Hudson, R. J. M. and Morel, F. M. M.: Distinguishing between extra- and intracellular iron in  
29 marine phytoplankton, *Limnol. Oceanogr.* 34: 1113-1120, doi:10.4319/lo.1989.34.6.1113,  
30 1989.

1 Johnson, K. et al.: Developing standards for dissolved iron in seawater, *Eos Trans. AGU*,  
2 88(11), 131–132, doi:10.1029/2007EO110003, 2007.

3 Kieffer, B., Arndt, N. T. and Weis, D.: A Bimodal Alkalic Shield Volcano on Skiff Bank: its  
4 Place in the Evolution of the Kerguelen Plateau, *J. Petrology*, 43(7), 1259-1286,  
5 doi:10.1093/petrology/43.7.1259, 2002.

6 King, P. et al.: Analysis of total and organic carbon and total nitrogen in settling oceanic  
7 particles and a marine sediment: an interlaboratory comparison, *Mar. Chem.*, 60, 203-216,  
8 doi: 10.1016/S0304-4203(97)00106-0, 1998.

9 Lam, P. J. and Bishop, J. K. B.: The continental margin is a key source of iron to the HNLC  
10 North Pacific Ocean, *Geophys. Res. Lett.*, 35, L07608, doi:10.1029/2008GL033294, 2008.

11 Lam, P. J., Bishop, J. K. B., Henning, C. C., Marcus, M. A., Waychunas, G. A., and Fung, I.  
12 Y.: Wintertime phytoplankton bloom in the subarctic Pacific supported by continental margin  
13 iron, *Glob. Biogeochem. Cycles*, 20, GB1006, doi:10.1029/2005GB002557, 2006.

14 Lamborg, C. H., Buesseler, K. O., and Lam, P. J.: Sinking fluxes of minor and trace elements  
15 in the North Pacific Ocean measured during the VERTIGO program, *Deep Sea Res. II*, 55  
16 (14–15), 1564–1577, doi:10.1016/j.dsr2.2008.04.012, 2008a.

17 Lamborg, C. H., Buesseler, K. O., Valdes, J., Bertrand, C. H., Bidigare, R., Manganini, S.,  
18 Pike, S., Steinberg, D., Trull, T., Wilson, S.: The flux of bio- and lithogenic material  
19 associated with sinking particles in the mesopelagic “Twilight Zone” of the northwest and  
20 north central Pacific Ocean, *Deep Sea Res. II*, doi:10.1016/j.dsr1012.2008.1004.1011, 2008b.

21 Lasbleiz, M., Leblanc, K., Blain, S., Ras, J., Cornet-Barthaux, V., Hélias Nunige, S., and  
22 Quéguiner, B.: Pigments, elemental composition (C, N, P, and Si), and stoichiometry of  
23 particulate matter in the naturally iron fertilized region of Kerguelen in the Southern Ocean,  
24 *Biogeosciences*, 11, 5931-5955, doi:10.5194/bg-11-5931-2014, 2014.Laurenceau-Cornec, E.  
25 C., Trull, T. W., Davies, D. M., Bray, S. G., Doran, J., Planchon, F., Carlotti, F., Jouandet,  
26 M.-P., Cavagna, A.-J., Waite, A. M., and Blain, S.: The relative importance of phytoplankton  
27 aggregates and zooplankton fecal pellets to carbon export: insights from free-drifting  
28 sediment trap deployments in naturally iron-fertilised waters near the Kerguelen Plateau,  
29 *Biogeosciences*, 12, 1007-1027, doi:10.5194/bg-12-1007-2015, 2015.Le Moigne F. A. C,  
30 Moore C. M., Sanders R. J., Villa-Alfageme M., Steigenberger S., and Achterberg E. P.:



1 Sequestration efficiency in the iron limited North Atlantic: Implications for iron supply mode  
2 to fertilized blooms, *Geophys. Res. Lett.*, 41, 4619–4627, doi:10.1002/2014GL060308, 2014.

3 Mackie, D. S., Peat, J. M., McTainsh, G. H., Boyd, P. W., and Hunter, K. A.: Soil abrasion  
4 and eolian dust production: Implications for iron partitioning and solubility, *Geochem.*  
5 *Geophys. Geosyst.*, 7, Q12Q03, doi:10.1029/2006GC001404, 2006.

6 Mackie, D. S., Boyd, P. W., McTainsh, G. H., Tindale, N. W., Westberry, T. K., and Hunter,  
7 K. A.: Biogeochemistry of iron in Australian dust: From eolian uplift to marine uptake,  
8 *Geochem. Geophys. Geosyst.*, 9, Q03Q08, doi:10.1029/2007GC001813, 2008.

9 Mahowald, N. M.: Anthropocene changes in desert area: Sensitivity to climate model  
10 predictions, *Geophys. Res. Lett.*, 34, L18817, doi:10.1029/2007GL030472, 2007.

11 Malits, A., Christaki, U., Obernosterer, I., and Weinbauer, M. G.: Enhanced viral production  
12 and virus-mediated mortality of bacterioplankton in a natural iron-fertilized bloom event  
13 above the Kerguelen Plateau, *Biogeosciences*, 11, 6841-6853, doi:10.5194/bg-11-6841-2014,  
14 2014.Marsay, C. M., Sedwick, P. N., Dinninman, M. S., Barrett, P. M., Mack, S. L. and  
15 McGillicuddy Jr, D. J.: Estimating the benthic efflux of dissolved iron on the Ross Sea  
16 continental shelf, *Geophys. Res. Lett.*, 41, doi:10.1002/2014GL061684, 2014.

17 Martin, J. H.: Glacial-interglacial CO<sub>2</sub> change: The iron hypothesis, *Paleoceanography*, 5(1),  
18 1–13, doi:10.1029/PA005i001p00001, 1990.

19 Measures, C. I., Landing, W. M., Brown, M. T., and Buck, C. S.: High-resolution Al and Fe  
20 data from the Atlantic Ocean CLIVAR-CO<sub>2</sub> Repeat Hydrography A16N transect: extensive  
21 linkages between atmospheric dust and upper ocean geochemistry, *Glob. Biogeochem.*  
22 *Cycles*, 22, GB1005, doi:10.1029/2007GB003042, 2008.

23 Mongin, M., Molina, E. and Trull, T. W.: Seasonality and scale of the Kerguelen plateau  
24 phytoplankton bloom: A remote sensing and modeling analysis of the influence of natural  
25 iron fertilization in the Southern Ocean, *Deep Sea Res. II*, 55(5-7): 880,  
26 doi:10.1016/j.dsr2.2007.12.039, 2008.

27 Moore, C. M., Hickman, A. E., Poulton, A. J., Seeyave, S. and Lucas, M. I.: Iron-light  
28 interactions during the CROZet natural iron bloom and EXport experiment (CROZEX) II:  
29 taxonomic responses and elemental stoichiometry, *Deep Sea Res. II*, 54 (18-20) 2066-2084,  
30 doi:10.1016/j.dsr2.2007.06.015, 2008.

1 Moore, J. K. and Doney, S. C.: Iron availability limits the ocean nitrogen inventory stabilizing  
2 feedbacks between marine denitrification and nitrogen fixation. *Glob. Biogeochem. Cycle* 21,  
3 GB2001, doi:10.1029/2006GB002762, 2007.

4 Morris P. J. and Charette M. A.: A synthesis of upper ocean carbon and dissolved iron  
5 budgets for Southern Ocean natural iron fertilisation studies, *Deep Sea Res. II*, 90, 147–157,  
6 doi:10.1016/j.dsr2.2013.02.001, 2013.

7 Mosseri, J., Quéguiner, B., Armand, L. and Cornet-Barthaux, V.: Impact of iron on silicon  
8 utilization by diatoms in the Southern Ocean: A case study of Si/N cycle decoupling in a  
9 naturally iron-enriched area, *Deep Sea Res. II*, 55, 801-819, doi: 10.1016/j.dsr2.2007.12.003,  
10 2008.

11 Nishioka, J., Ono, T., Saito, H., Sakaoka, K., and Yoshimura, T.: Oceanic iron supply  
12 mechanisms which support the spring diatom bloom in the Oyashio region, western subarctic  
13 Pacific, *J. Geophys. Res.*, 116, C02021, doi:10.1029/2010JC006321, 2011.

14 Obata, H., Karatani, H. and Nakayama, E.: Automated determination of iron in seawater by  
15 chelating resin concentration and chemiluminescence detection, *Anal. Chem.*, 5, 1524-1528,  
16 doi: 10.1021/ac00059a007, 1993.

17 Osborn, T.R.: Estimates of the local rate of vertical diffusion from dissipation measurements,  
18 *Journal of Physical Oceanography* 10, 83–89, doi:10.1175/1520-  
19 0485(1980)010<0083:EOTLRO>2.0.CO;2, 1980.

20 Park, Y.-H., Fuda, J.-L., Durand, I. and Naveira Garabato, A.C.: Internal tides and vertical  
21 mixing over the Kerguelen Plateau, *Deep Sea Res. II*, 55(5-7), 582-593,  
22 doi:10.1016/j.dsr2.2007.12.027, 2008a.

23 Park, Y.-H., Roquet, F., Durand, I. and Fuda, J.-L.: Large-scale circulation over and around  
24 the Northern Kerguelen Plateau, *Deep Sea Res. II*, 55(5-7), 566-581,  
25 doi:10.1016/j.dsr2.2007.12.030, 2008b.

26 Park, Y.-H., Durand, I., Kestenare, E., Rougier, G., Zhou, M., d'Ovidio, F., Cotté, C., and Lee,  
27 J.-H.: Polar Front around the Kerguelen Islands: An up-to-date determination and associated  
28 circulation of surface/subsurface waters, *J. Geophys. Res. Oceans*, 119,  
29 doi:10.1002/2014JC010061, 2014a.

1 Park, Y.-H., Lee, J.-H., Durand, I., and Hong, C.-S.: Validation of Thorpe-scale-derived  
2 vertical diffusivities against microstructure measurements in the Kerguelen region,  
3 *Biogeosciences*, 11, 6927-6937, doi:10.5194/bg-11-6927-2014, 2014. Planchon, F., Ballas, D.,  
4 Cavagna, A.-J., Bowie, A. R., Davies, D., Trull, T., Laurenceau, E., Van Der Merwe, P., and  
5 Dehairs, F.: Carbon export in the naturally iron-fertilized Kerguelen area of the Southern  
6 Ocean based on the  $^{234}\text{Th}$  approach, *Biogeosciences Discuss.*, 11, 15991-16032,  
7 doi:10.5194/bgd-11-15991-2014, 2014.

8 Planquette, H. and Sherrell, R. M.: Sampling for particulate trace element determination  
9 using water sampling bottles: methodology and comparison to in situ pumps, *Limnol.*  
10 *Oceanogr. Methods*, 10, 367–388, doi:10.4319/lom.2012.10.367, 2012.

11 Planquette H. et al.: Dissolved iron in the vicinity of the Crozet Islands, Southern Ocean,  
12 *Deep Sea Res. II*, 54(18-20), 1999-2019, doi:10.1016/j.dsr2.2007.06.019, 2007.

13 Planquette H., Fones G. R., Statham P. J., and Morris P. J.: Origin of iron and aluminium in  
14 large particles (>53  $\mu\text{m}$ ) in the Crozet region, Southern Ocean, *Mar. Chem.*, 115, 31–42, doi:  
15 10.1016/j.marchem.2009.06.002, 2009.

16 Planquette, H., Sanders, R. R., Statham, P. J., Morris, P. J., and Fones, G. R.: Fluxes of  
17 particulate iron from the upper ocean around the Crozet Islands: A naturally iron-fertilized  
18 environment in the Southern Ocean, *Glob. Biogeochem. Cycles*, 25, GB2011,  
19 doi:10.1029/2010GB003789, 2011.

20 Planquette, H., Sherrell R. M., Stammerjohn, S., and Field M. P.: Particulate iron delivery to  
21 the water column of the Amundsen Sea, Antarctica, *Mar. Chem.*, 153, 15–30,  
22 doi:10.1016/j.marchem.2013.04.006, 2013.

23 Pollard, R. T. et al.: Southern Ocean deep-water carbon export enhanced by natural iron  
24 fertilization, *Nature*, 457, 577–580, doi:10.1038/nature07716, 2009.

25 Price, N. M. and Morel, F. M. M.: Biological cycling of iron in the ocean. In: “Metal Ions in  
26 Biological Systems”, Vol. 35, Iron Transport and Storage in Micro-organisms, Plants and  
27 Animals. Marcel Dekker, New York, pp. 1-36, 1998.

28 Prospero, J. M., Ginoux, P., Torres, O., Nicholson, S. E., and Gill, T. E.: Environmental  
29 characterization of global sources of atmospheric soil dust identified with the Nimbus 7 Total  
30 Ozone Mapping Spectrometer (TOMS) absorbing aerosol product, *Rev. Geophys.*, 40 (1),  
31 1002, doi:doi:10.1029/2000RG000095, 2002.

1 Qu erou , F., Sarthou, G., Planquette, H. F., Bucciarelli, E., Chever, F., van der Merwe, P.,  
2 Lannuzel, D., Townsend, A. T., Cheize, M., Blain, S., d'Ovidio, F., and Bowie, A. R.: High  
3 variability of dissolved iron concentrations in the vicinity of Kerguelen Island (Southern  
4 Ocean), *Biogeosciences Discuss.*, 12, 231-270, doi:10.5194/bgd-12-231-2015, 2015. Roquet,  
5 F., Park, Y.-H., Guinet, C., Bailleul, F., and Charrassin, J.-B.: Observations of the Fawn  
6 Trough Current over the Kerguelen Plateau from instrumented elephant seals, *J. Mar. Sys.*,  
7 doi:10.1016/j.jmarsys.2008.11.017, 2009.

8 Rosso, I., et al.: Vertical transport in the ocean due to sub-mesoscale structures: Impacts in the  
9 Kerguelen region, *Ocean Model.*, doi:10.1016/j.ocemod.2014.05.001, 2014.

10 Sanial, V., van Beek, P., Lansard, B., Souhaut, M., Kestenare, E., d'Ovidio, F., Zhou, M., and  
11 Blain, S.: Use of Ra isotopes to deduce rapid transfer of sediment-derived inputs off  
12 Kerguelen, *Biogeosciences*, 12, 1415-1430, doi:10.5194/bg-12-1415-2015, 2015. Sarmiento,  
13 J. L., Gruber, N.: Carbon Cycle. Chapter 8 in: "Ocean Biogeochemical Dynamics", Princeton  
14 University Press, Princeton (USA), pp. 318-358, ISBN: 9780691017075, 2006.

15 Sarthou, G., Baker, A. R., Blain, S., Achterberg, E. P., Boye, M., Bowie, A. R., Croot, P.,  
16 Laan, P., de Baar, H. J. W., Jickells, T. D. and Worsfold, P. J.: Atmospheric iron deposition  
17 and sea-surface dissolved iron concentrations in the eastern Atlantic Ocean, *Deep Sea Res. I*,  
18 50, 1339–1352, doi:10.1016/S0967-0637(03)00126-2, 2003.

19 Sarthou, G., Vincent, D., Christaki, U., Obernosterer, I., Timmermans, K.R. and Brussaard,  
20 C.P.D.: The fate of biogenic iron during a phytoplankton bloom induced by natural  
21 fertilisation: Impact of copepod grazing, *Deep Sea Res. II*, 55(5-7), 734,  
22 doi:10.1016/j.dsr2.2007.12.033, 2008.

23 Savoye, N., Trull, T. W., Jacquet, S. H. M., Navez, J. and Dehairs, F.: <sup>234</sup>Th-based export  
24 fluxes during a natural iron fertilization experiment in the Southern Ocean (KEOPS), *Deep*  
25 *Sea Res. II*, 55(5-7): 841, doi:10.1016/j.dsr2.2007.12.036, 2008.

26 Schlitzer, R.: Carbon export fluxes in the Southern Ocean: results from inverse modelling and  
27 comparison with satellite-based estimates, *Deep Sea Res. II*, 49, 1623–1644,  
28 doi:10.1016/S0967-0645(02)00004-8, 2002.

29 Schneider, B., Schlitzer, R., Fischer, G., and Nothig, E.-M.: Depth dependent elemental  
30 compositions of particulate organic matter (POM) in the ocean, *Glob. Biogeochem. Cycles*,  
31 17(2), doi:10.1029/2002GB001871, 2003.

1 Schroth, A. W., Crusius, J., Sholkovitz, E. R., and Bostick, B. C.: Iron solubility driven by  
2 speciation in dust sources to the ocean, *Nat. Geosci.* 2, 337–340, doi: doi:10.1038/ngeo501,  
3 2009.

4 SCOR Working Group: GEOTRACES – An international study of the global marine  
5 biogeochemical cycles of trace elements and their isotopes, *Chem. Erde*, 67, 85–131,  
6 doi:10.1016/j.chemer.2007.02.001, 2007.

7 Sedwick, P. N., Sholkovitz, E. R., and Church, T. M.: Impact of anthropogenic combustion  
8 emissions on the fractional solubility of aerosol iron: Evidence from the Sargasso Sea,  
9 *Geochem. Geophys. Geosyst.*, 8, Q10Q06, doi:10.1029/2007GC001586, 2007.

10 Shaked, Y. and Lis, H.: Disassembling Iron Availability to Phytoplankton. *Front. Microbiol.*  
11 3:123, doi:10.3389/fmicb.2012.00123, 2012.

12 Sherrell, R. M. and Boyle, E. A.: The trace metal composition of suspended particles in the  
13 oceanic water column near Bermuda, *Earth Planet. Sci. Lett.*, 111 (1), 155–174,  
14 doi:10.1016/0012-821X(92)90176-V, 1992.

15 Shih, L. H., Koseff, J. R., Ivey, G. N., and Ferziger, J. H.: Parameterization of turbulent fluxes  
16 and scales using homogeneous sheared stably stratified turbulence simulations, *Journal of*  
17 *Fluid Mechanics*, 525, 193–214, doi:10.1017/S0022112004002587, 2005.

18 Sokolov, S. and Rintoul, S. R.: Circumpolar structure and distribution of the Antarctic  
19 Circumpolar Current fronts: 1. Mean circumpolar paths, *J. Geophys. Res.*, 114, C11018,  
20 doi:10.1029/2008JC005108, 2009.

21 Strzepek, R. F., Maldonado, M. T., Higgins, J. L., Hall, J., Safi, K., Wilhelm, S. W., and  
22 Boyd, P.W.: Spinning the “Ferrous Wheel”: the importance of the microbial community in an  
23 iron budget during the FeCycle experiment, *Glob. Biogeochem. Cycles*, 19, GB4S26,  
24 doi:10.1029/2005GB002490, 2005

25 Sunda, W. G. and Huntsman, S. A.: Iron uptake and growth limitation in oceanic and coastal  
26 phytoplankton, *Mar. Chem.*, 50: 189-206, doi:10.1016/0304-4203(95)00035-P, 1995.

27 Tagliabue, A., Bopp, L., and Aumont, O.: Evaluating the importance of atmospheric and  
28 sedimentary iron sources to Southern Ocean biogeochemistry, *Geophys. Res. Lett.*, 36,  
29 L13601, doi:10.1029/2009GL038914, 2009.

1 Tagliabue, A., Sallée, J.-B., Bowie, A. R., Lévy, M., Swart, S., and Boyd, P. W.: Surface-  
2 water iron supplies in the Southern Ocean sustained by deep winter mixing, *Nat. Geosci.*, 7,  
3 314–320, doi:10.1038/ngeo2101, 2014.

4 Tang D. G. and Morel F. M. M.: Distinguishing between cellular and Fe-oxide-associated  
5 trace elements in phytoplankton, *Mar. Chem.*, 98, 18-30, doi:10.1016/j.marchem.2005.06.003,  
6 2006.

7 Taylor, S. R. and McLennan, S. M.: The geochemical evolution of the continental crust. *Rev.*  
8 *Geophys.*, 33(2), 241-265, doi:10.1029/95RG00262, 1995.

9 Thuróczy, C.-E., Alderkamp, A.-C., Laan, P., Gerringa, L. J. A., de Baar, H. J. W., Arrigo, K.  
10 R.: Key role of organic complexation of iron in sustaining phytoplankton blooms in the Pine  
11 Island and Amundsen Polynyas (Southern Ocean), *DSR II*, 71-76, 49-60,  
12 doi:10.1016/j.dsr2.2012.03.009, 2012.

13 Tortell, P. D., Maldonado, M. T., and Price, N. M.: The role of heterotrophic bacteria in iron-  
14 limited ocean ecosystems, *Nature*, 383, 330–332, doi:10.1038/383330a0, 1996.

15 Trull, T. W., Davies, D., and Casciotti, K.: Insights into nutrient assimilation and export in  
16 naturally iron-fertilized waters of the Southern Ocean from nitrogen, carbon and oxygen  
17 isotopes, *Deep Sea Res. II*, 55(5-7), 820-840, doi:10.1016/j.dsr2.2007.12.035, 2008.

18 Trull, T. W., Davies, D. M., Dehairs, F., Cavagna, A.-J., Lasbleiz, M., Laurenceau-Cornec, E.  
19 C., d'Ovidio, F., Planchon, F., Leblanc, K., Quéguiner, B., and Blain, S.: Chemometric  
20 perspectives on plankton community responses to natural iron fertilisation over and  
21 downstream of the Kerguelen Plateau in the Southern Ocean, *Biogeosciences*, 12, 1029-1056,  
22 doi:10.5194/bg-12-1029-2015, 2015. Twining, B. S., Baines, S. B., Fisher, N. S., and Landry  
23 M. R.: Cellular iron contents of plankton during the Southern Ocean Iron Experiment  
24 (SOFeX), *Deep Sea Res. I*, 51, 1827– 1850, doi:10.1016/j.dsr.2004.08.007, 2004.

25 van Beek, P., Bourquin, M., Reyss, J. L., Souhaut, M., Charette, M. A., and Jeandel, C.:  
26 Radium isotopes to investigate the water mass pathways on the Kerguelen Plateau (Southern  
27 Ocean), *Deep Sea Res. II*, 55, 622-637, doi:10.1016/j.dsr2.2007.12.025, 2008.

28 van der Merwe, P., Bowie, A. R., Quéroué, F., Armand, L., Blain, S., Chever, F., Davies, D.,  
29 Dehairs, F., Planchon, F., Sarthou, G., Townsend, A. T., and Trull, T. W.: Sourcing the iron in  
30 the naturally fertilised bloom around the Kerguelen Plateau: particulate trace metal dynamics,  
31 *Biogeosciences*, 12, 739-755, doi:10.5194/bg-12-739-2015, 2015. Wadley, M. R., Jickells, T.

1 D., and Heywood, K. J.: The role of iron sources and transport for Southern Ocean  
2 productivity, *Deep Sea Res. I*, 87, 82-94, doi:10.1016/j.dsr.2014.02.003, 2014.

3 Wagener, T., Guieu, C., Losno, R., Bonnet, S., and Mahowald, N.: Revisiting atmospheric  
4 dust export to the southern hemisphere ocean: biogeochemical implication, *Glob.*  
5 *Biogeochem. Cycles*, 22, GB2006, 1-13, doi:10.1029/2007GB002984, 2008.

6 Wedepohl, K. H.: The composition of the continental crust, *Geochim. Cosmochim. Acta*, 59,  
7 1217–1232, doi:10.1016/0016-7037(95)00038-2, 1995.

8 Westberry, T. K., Behrenfeld, M. J., Milligan, A. J., and Doney, S. C.: Retrospective satellite  
9 ocean color analysis of purposeful and natural ocean iron fertilization, *Deep Sea Res. I*, 73, 1-  
10 16, doi:10.1016/j.dsr.2012.11.010, 2013.

11 Zhang, Y., Lacan, F., and Jeandel, C.: Dissolved rare earth elements tracing lithogenic inputs  
12 over the Kerguelen Plateau (Southern Ocean), *Deep Sea Res. II*, 55, 638-652,  
13 doi:10.1016/j.dsr2.2007.12.029, 2008.

14 Zhou, M., Zhu, Y., Dorland, R. D., and Measures, C. I.: Dynamics of the current system in the  
15 southern Drake Passage, *Deep Sea Res. I*, 57, 1039-1048, doi:10.1016/j.dsr.2010.05.012,  
16 2014.

17 Zhou, M., Zhu, Y., d'Ovidio, F., Park, Y.-H., Durand, I., Kestenare, E., Sanial, V., Van-Beek,  
18 P., Quéguiner, B., Carlotti, F., and Blain, S.: Surface currents and upwelling in Kerguelen  
19 Plateau regions, *Biogeosciences Discuss.*, 11, 6845-6876, doi:10.5194/bgd-11-6845-2014,  
20 2014.

21

## 1 **Figure captions**

2 Figure 1. (a) The location of the KEOPS-2 study in the Indian sector of the Southern Ocean  
3 showing bathymetry around the Kerguelen archipelago. Our biogeochemical iron budgets  
4 focus on three process stations (open black circles): reference R-2 (50°2' S, 66°4' E), plateau  
5 A3 (50°4' S, 72°0' E) and plume E (48°3' S, 72°1' E). Black dots mark the positions of the  
6 other stations visited, including N-S and E-W survey transects at the start of the KEOPS-2  
7 expedition. (b) A schematic of the mean regional circulation of surface/subsurface waters  
8 around the Kerguelen archipelago, indicating circumpolar Southern Ocean fronts, locations of  
9 stations conducted along N-S and E-W transects, and pathways and origins of different water  
10 masses flowing on the plateau and offshore into the plume. The abbreviations are Antarctic  
11 Surface Water (AASW), Polar Frontal Surface Water (PFSW), Subantarctic Surface Water  
12 (SASW), and Subtropical Surface Water (STSW), subantarctic front (SAF), polar front (PF)  
13 (reproduced with permission from Park et al. (2014a), courtesy of Isabelle Durand and  
14 Young-Hyang Park, LOCEAN/DMPA, MNHN, Paris).

15 Figure 2. MODIS ocean-colour satellite images showing the development of the plateau and  
16 plume blooms during the KEOPS-2 study. Surface chlorophyll ( $\mu\text{g L}^{-1}$ ) biomass is shown for  
17 the nearest clear sky day to the final sampling day at stations R-2 (panel a), A3-2 (panel b)  
18 and E-5 (panel c). The polar front is shown as a black dashed line in panels b and c. Trull et  
19 al. (2015) discuss the timing of the stations relative to bloom development.

20 Figure 3(a). Vertical profiles of dissolved iron (dFe) and particulate iron (pFe), potential  
21 temperature, salinity and nitrate at reference station R-2. The seafloor depth at 2528 m is  
22 shown. (b, c) Vertical profiles of dFe and pFe, potential temperature, salinity and nitrate at  
23 plateau stations A3-1 (panel b) and A3-2 (panel c). The seafloor depth at ~530 m is shown.  
24 Note different scales for dFe and pFe compared to R-2 and E stations. (d, e, f) Vertical  
25 profiles of dFe and pFe, potential temperature, salinity and nitrate at plume stations E1 (panel  
26 d), E3 (panel e) and E5 (panel f). The seafloor depth ranging from 1905 m (E3) to 2057 m  
27 (E1) is shown.

28 Figure 4. (a) Comparison of dFe and pFe at reference stations for KEOPS-1 (station C11,  
29 open blue diamonds) and KEOPS-2 (station R-2, closed red squares) studies. The water  
30 depths were 3110 m at C11 and 2530 m at R-2. (b) Comparison of dFe and pFe at A3 plateau  
31 stations for KEOPS-1 (open symbols) and KEOPS-2 (closed symbols) studies. Data are



1 shown for all visits to A3 on both KEOPS cruises. Note difference in scale for dFe and pFe  
2 between (a) and (b).

3 Figure 5. Vertical profiles of Fe/C ratios in suspended (ISP) and sinking (P-trap) particles.  
4 Solid symbols indicate “total” Fe/C (i.e., ratio of biogenic + lithogenic Fe over POC) and  
5 joined open symbols indicate  $Fe_{bio}/C$  (i.e., ratio of biogenic Fe only over POC; calculated  
6 using P as a normaliser). The asterisk markers (\*) show the export “total” Fe/C ratio (P-traps).  
7 Note the different scale on the x-axis for Fe/C at A3 stations.

8 Figure 6. A comparison of export fluxes of pFe versus POC in sinking particles for natural  
9 iron fertilisation studies in the Southern Ocean. For details of the sampling methods, refer to  
10 Table 2 and the original articles. The lines indicate Fe/C ratios for Fe limited (black dashed)  
11 and Fe replete (black solid) phytoplankton (Twining et al., 2004), and the mean mixed layer  
12 intracellular Fe/C ratios at stations A3-2 (orange dashed) and E5 (orange solid) on KEOPS-2  
13 (taken from Table 1). FeCycle-II had complex biogeochemical dynamics due to a storm event  
14 and subsequent deep water mixing (during sediment trap deployment at their station A3),  
15 splitting the study into two phases (“eddy centre” and “eddy periphery”). To aid interpretation  
16 of Fe/C export data in the context of iron fertilisation, only data from the pseudo Lagrangian  
17 phase 1 (i.e., deployments A1 and A2 during bloom development and export) from that study  
18 is included in this plot (Ellwood et al., 2014).

19 Figure 7. Biogeochemical iron budgets for the reference (R-2, panel a), plateau (A3-2, panel  
20 b) and plume (E-5, panel c) stations. Iron pools are given in  $\mu\text{mol m}^{-2}$  and iron fluxes in  $\text{nmol}$   
21  $\text{m}^{-2} \text{d}^{-1}$ . Iron sources are shown as blue arrows, sinks as red arrows and the green arrows  
22 indicate biological Fe cycling. The size of the arrows is roughly proportional to the magnitude  
23 of the Fe fluxes, with major fluxes shown as bold underlined text..

24

1 Table 1. Summary of iron standing stocks and fluxes for the upper mixed layer at KEOPS-2 process station sites R-2 (reference), A3 (plateau)  
 2 and E (plume). For full details of the calculations, see text. Error bounds are provided where available. Due to logistical constraints resulting  
 3 in missing data at some stations, we will focus on R-2, A3-2 and E-5 in the discussion. Data for stations A3-1, E-1 and E-3 are given to  
 4 provide a context for spatial and temporal changes in the pools and fluxes during KEOPS-2.

5

<b>Region</b>	<b>Reference</b>	<b>Plateau</b>		<b>Plume</b>		
Station	R-2	A3-1	A3-2	E-1	E-3	E-5
Location	50°21.53' S 66°42.44' E	50°37.88' S 72°04.99' E	50°37.47' S 72°03.35' E	48°27.44' S 72°11.26' E	48°42.13' S 71°58.01' E	48°24.69' S 71°53.99' E
Mixed layer depth (m) <sup>1</sup>	76	165	123	64	32	39
Bottom depth (m)	2528	533	530	2057	1905	1920
<b><i>Iron pools, integrated over the mixed layer (<math>\mu\text{mol m}^{-2}</math>, unless otherwise stated)</i></b>						
dFe	7 ± 1	54 ± 10	21 ± 4	n.d. <sup>2</sup>	12 ± 0	2 ± 0
pFe	43 ± 0	1392 ± 195	401 ± 52	117 ± 1	n.d. <sup>3</sup>	61 ± 1
Biogenic pFe	9	13	14	11	n.d.	9
Lithogenic pFe	12	892	265	33	n.d.	9
POC ( $\text{mmol m}^{-2}$ )	124 ± 11	239 ± 33	274 ± 24	198 ± 10	n.d.	150 ± 12
<b><i>Iron fluxes (<math>\text{nmol m}^{-2} \text{d}^{-1}</math>, unless otherwise stated)</i></b>						
(a) Diffusion	2	42	93	n.d.	1	0.5
(b) Upwelling	35	200	250	n.d.	330	140
(c) Entrainment	57	769	769	n.d.	330	330
(d) Total vertical dFe supply [a+b+c]	94	1011	1112	n.d.	661	471
(e) Lateral advective dFe supply	0	180		2400±600		
Ratio of lateral-to-vertical supply [e/d]	0	0.2		4-5		

Atmospheric total Fe deposition	500 ± 390					
(f) Atmospheric soluble Fe deposition	50 ± 39					
Downward total pFe export flux	1302 ± 586 <sup>4</sup>	n.d.	5746 ± 1198	4579 ± 1376	1890 ± 286	895 ± 358
(g) Downward non-lithogenic pFe export flux			2797 ± 583			541 ± 216
Downward POC export (mmol m <sup>-2</sup> d <sup>-1</sup> )	1.8 ± 0.9 <sup>5</sup>	n.d.	2.2 ± 0.7	7.0 ± 2.3	4.9 ± 1.5	2.0 ± 1.0
(h) Iron uptake <sup>6</sup>	40 ± 6	2528 ± 704	1120 ± 389	n.d.	743 ± 194	1745 ± 350
(i) Iron remineralization <sup>7</sup>	10 ± 2	19 ± 6	71 ± 12	27 ± 2	23 ± 2	31 ± 2
<i>Fe/C ratios (mmol mol<sup>-1</sup>)</i>						
(j) Mixed layer Fe/C cellular uptake ratio <sup>8</sup>	n.d.	n.d.	0.007 ± 0.004	n.d.	n.d.	0.021 ± 0.002
Suspended mixed layer particulate “total” Fe/C ratio <sup>8</sup>	0.2 ± 0.1	3.3 ± 0.4	1.5 ± 0.2	0.5 ± 0.1	n.d.	0.4 ± 0.1
Sinking “total” Fe/C export ratio	n.d.	n.d.	2.6 ± 1.0	0.7 ± 0.5	0.4 ± 0.3	0.5 ± 0.1
<i>Iron supply vs demand (for reference R-2, plateau A3-2 and plume E-5 stations ONLY) (nmol m<sup>-2</sup> d<sup>-1</sup>)</i>						
Total iron supply from ‘new’ sources [d+e+f] <sup>9</sup>	144		1342			2921
(k) Additional iron requirement to balance the dissolved budget [d+e+f-h+i] <sup>10</sup>	114		293			1207
(l) Biological uptake of ‘new’ iron [d+e+f-g] <sup>11</sup>	-1158		-1455			2380
fe ratio [l/h] <sup>12</sup>						1.4
Fe ratio [g/h] <sup>12</sup>						0.3
<i>Estimated vs observed production (mmol C m<sup>-2</sup> d<sup>-1</sup>)</i>						
Potential new primary production [l/j] <sup>13</sup>						132
Observed net primary production <sup>14</sup>	11 ± 0	n.d.	158 ± 15	44 ± 4	57 ± 8	79 ± 9

1

1 n.d. = no data

2 <sup>1</sup> The mixed layer depths were calculated on the density plane to allow for heave (internal tides driven by topography) and other localised  
3 events

4 <sup>2</sup> Due to logistical reasons there was no TMR cast for dFe at station E-1

5 <sup>3</sup> Due to ISP failure, there were no mixed layer samples for pFe at station E-3

6 <sup>4</sup> The P-trap was lost at R-2. We therefore estimated the pFe export flux using the <sup>234</sup>Th flux in suspended particles at 200 m ( $449 \pm 203$  dpm  
7  $\text{m}^{-2} \text{d}^{-1}$ ; from Table 1 in Planchon et al., 2014) and a mean Fe/Th ratio collected in the upper 200 m above the trap ( $2.9 \pm 1.3$  nmol dpm<sup>-1</sup>). This  
8 estimation method will reflect the integrated Fe export over the previous ~30 days, rather than an instantaneous flux at the time of sampling.  
9 Since this was a reference site, with low phytoplankton abundance, the longer time period probably has a minimal effect upon interpretation of  
10 the data

11 <sup>5</sup> Estimated using the <sup>234</sup>Th flux and Fe/C ratio in suspended particles at 200 m

12 <sup>6</sup> For stations R-2, A3-1, E-1 and E-3, seawater for iron uptake experiments were conducted for small cells filtered through a 25  $\mu\text{m}$  mesh.  
13 This size-fraction represented between 77% and 91% of the total POC pool. At stations A3-2 and E-5, we also used unfiltered seawater for our  
14 uptake experiments. Similar results were obtained for both the 0.2-25  $\mu\text{m}$  and unfiltered fractions at station A3-2

15 <sup>7</sup> Includes bacterial and mesozooplankton contributions

16 <sup>8</sup> Mean of all samples collected in the mixed layer

17 <sup>9</sup> Assumes only the soluble iron atmospheric supply is available (see text)

18 <sup>10</sup> A negative value indicates an additional iron requirement

19 <sup>11</sup> At stations R-2 and A3-2, the negative values most likely occurred due to differences in the timescales of observations and calculations of  
20 fluxes (parameters were decoupled in time). The iron budget was based on an 'instantaneous picture' of different fluxes that were not strictly  
21 measured at the same time (i.e., export fluxes operated on a different timeframe to the iron supply (vertical, lateral and atmospheric) and were  
22 very large at R-2 and A3-2

23 <sup>12</sup>  $f_e$  = uptake of new/uptake of new + regenerated iron and  $F_e$  = biogenic iron export/uptake of new + regenerated iron [Boyd et al., 2005].  
24 Note the  $f_e$  and  $F_e$  ratios have considerable plasticity due to uncertainties in the lithogenic vs biogenic fraction of exported particulate iron,  
25 and the missing iron source at A3-2

- 1 <sup>13</sup> Calculated using the biological uptake of 'new' iron (k) and molar Fe/C cellular uptake ratio (j)
- 2 <sup>14</sup> Net primary production (NPP) integrated within the euphotic zone down to 1% PAR, based on <sup>13</sup>C incorporation (Cavagna et al., 2014)

1 Table 2. Fluxes of iron and carbon exported in sinking particles (trap deployed at 200 m) and  
 2 ratio of Fe/C in sinking (traps) and suspended mixed layer (ISP) particles at stations A3-2 and  
 3 E-stations. There was no successful trap deployment at station R-2. A comparison to previous  
 4 studies is provided.

Site	PFe flux ( $\mu\text{mol m}^{-2} \text{d}^{-1}$ )		POC flux ( $\text{mmol m}^{-2} \text{d}^{-1}$ )		Fe/C (sinking) ( $\text{mmol mol}^{-1}$ )		Fe/C (suspended) ( $\text{mmol mol}^{-1}$ )
	mean	stdev	mean	stdev	mean	stdev	mean
<b>KEOPS-2</b>							
A3-2	5.75	1.20	2.23	0.68	2.57	0.97	1.51
E-1	4.58	1.38	7.02	2.28	0.65	0.52	0.49
E-3	1.89	0.29	4.87	1.54	0.39	0.29	0.39
E-5	0.90	0.36	2.00	1.00	0.45	0.13	0.33
<b>KEOPS-1</b> <sup>1</sup>							
A3-initial	0.33	0.05	3.60	0.43	0.09		
A3-final	0.20	0.02	1.36	0.39	0.15		
C5	1.51	0.32	1.57	0.08	0.96		
<b>CROZEX</b> <sup>2</sup>							
North	0.84		15.9		2.55		0.69
South	0.23		12.9		0.57		0.31
<b>SAZ-Sense</b> <sup>3</sup>							
P1	0.17	0.09	3.34	1.81	0.05	0.04	0.04
P2	0.07	0.01	2.11	0.88	0.04	0.02	0.06
P3	0.21	0.05	0.86	0.38	0.25	0.13	0.03
<b>FeCycle-I</b> <sup>4</sup>							
F1-80 m	0.22	0.03	n.d.		n.d.		0.04
F1-120 m	0.36	0.05	2.09	0.03	0.17		
F2-80 m	0.55	0.06	2.51	0.17	0.22		
F2-120 m	0.35	0.03	2.10	0.01	0.17		
<b>FeCycle-II</b> <sup>5</sup>							
A1-100 m	5.0	0.7	11		0.45		0.78
A1-200 m	7.3	1.6	5.8		1.26		
A2-100 m	10	1.0	42		0.24		1.12
A2-200 m	10	9	6.8	1.8	1.47		
A3-100 m	17	2	12	2	1.42		0.63
A3-200 m	10	1	14		0.71		
A4-100 m	20	8	9.3	0.9	2.15		0.86
A4-200 m	15	6	6.1	1.8	2.46		
<b>Other literature data</b>							
Mixed plankton assemblages <sup>6</sup>							0.01-0.05
Iron limited algae <sup>7</sup>							0.01
Iron replete algae <sup>7</sup>							0.02-0.05
Southern Ocean synthesis <sup>8</sup>					0.01-0.06		

1

2 n.d. = no data

3 <sup>1</sup> Data for particles >0.2  $\mu\text{m}$  (Blain et al., 2007; Bowie et al., unpublished data)

4 <sup>2</sup> Data for >53  $\mu\text{m}$  particles only (Planquette et al., 2011). Downward Fe fluxes were  
5 estimated from samples collected from in situ pumps using <sup>234</sup>Th depletions and Fe/Th ratios  
6 in sinking particles. Waters to the north of Crozet Island were “downstream” of the islands  
7 and iron fertilised, whilst those to the south were “upstream” HNLC conditions. The Fe/C  
8 from bioassay culturing experiments conducted during CROZEX was 0.25  $\text{mmol mol}^{-1}$   
9 (Moore et al., 2008)

10 <sup>3</sup> Data for particles >1  $\mu\text{m}$  (Bowie et al., 2009)

11 <sup>4</sup> Data for particles >0.4  $\mu\text{m}$  (Frew et al., 2006). Only 1 mixed layer Fe/C ratio was reported.  
12 The biogenic Fe/C mixed layer ratio was estimated to be 0.004-0.012  $\text{mmol mol}^{-1}$

13 <sup>5</sup> Data for particles >0.4  $\mu\text{m}$ , except deployment A1 (>2  $\mu\text{m}$ ) (Ellwood et al., 2014). The  
14 mixed layer Fe/C ratios were calculated from Table 4 using the sediment traps deployment  
15 periods reported in Table 3 in the original publication

16 <sup>6</sup> Estimates of Fe/C for diatoms and whole plankton assemblages compiled by de Baar et al.  
17 (2008), with optimal ratios for growth tending towards the upper end of the range

18 <sup>7</sup> Intracellular ratio reported for HNLC polar water south of New Zealand during SOFeX  
19 (Twining et al., 2004)

20 <sup>8</sup> Ratio of dFe supply to POC export, synthesis by Morris and Charette (2013)

21

1 Table 3. Iron regeneration rates based on bacterivore and herbivore contributions.

2

Site	Bacterial ( $\text{pmol L}^{-1} \text{d}^{-1}$ )	Mesozooplankton ( $\text{pmol L}^{-1} \text{d}^{-1}$ )	Total Fe regeneration ( $\text{pmol L}^{-1} \text{d}^{-1}$ )	% bacterial contribution	Total integrated mixed layer Fe regeneration ( $\text{nmol m}^{-2} \text{d}^{-1}$ )
R-2	$0.06 \pm 0.01$	0.04	0.10	61	10
A3-1	$0.10 \pm 0.03$	0.02	0.12	87	19
A3-2	$0.43 \pm 0.07$	0.03	0.46	93	71
E-1	$0.33 \pm 0.02$	0.04	0.37	88	27
E-3	$0.54 \pm 0.04$	0.06	0.60	90	23
E-5	$0.59 \pm 0.03$	0.08	0.67	88	31

3



Figure 1

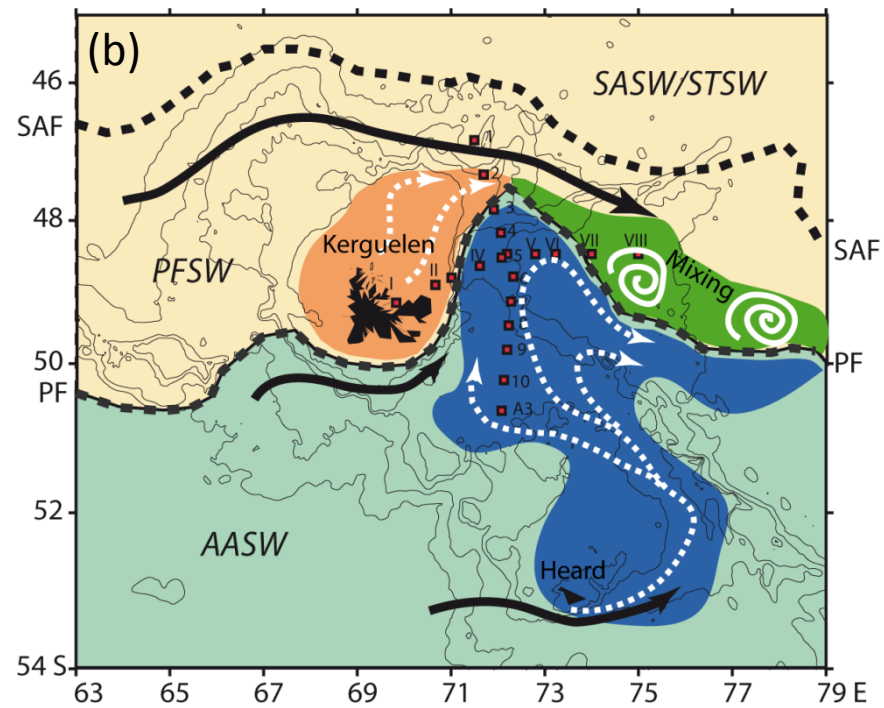
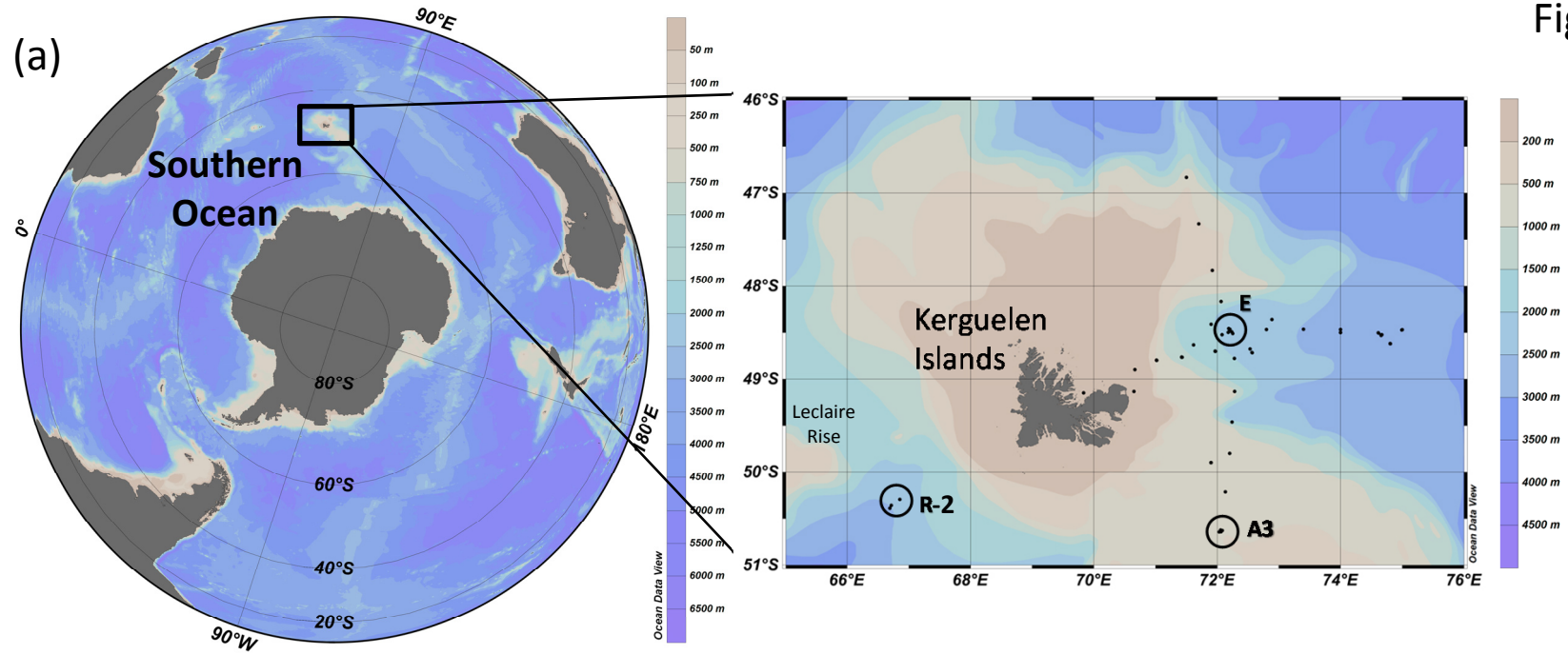


Figure 2

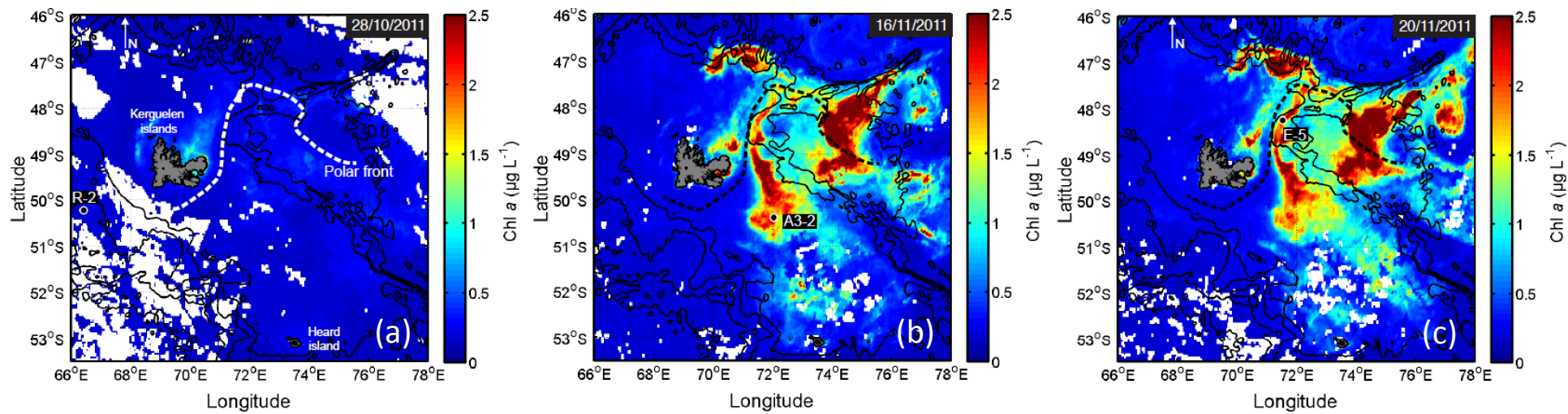


Figure 3a

### R-2 (reference)

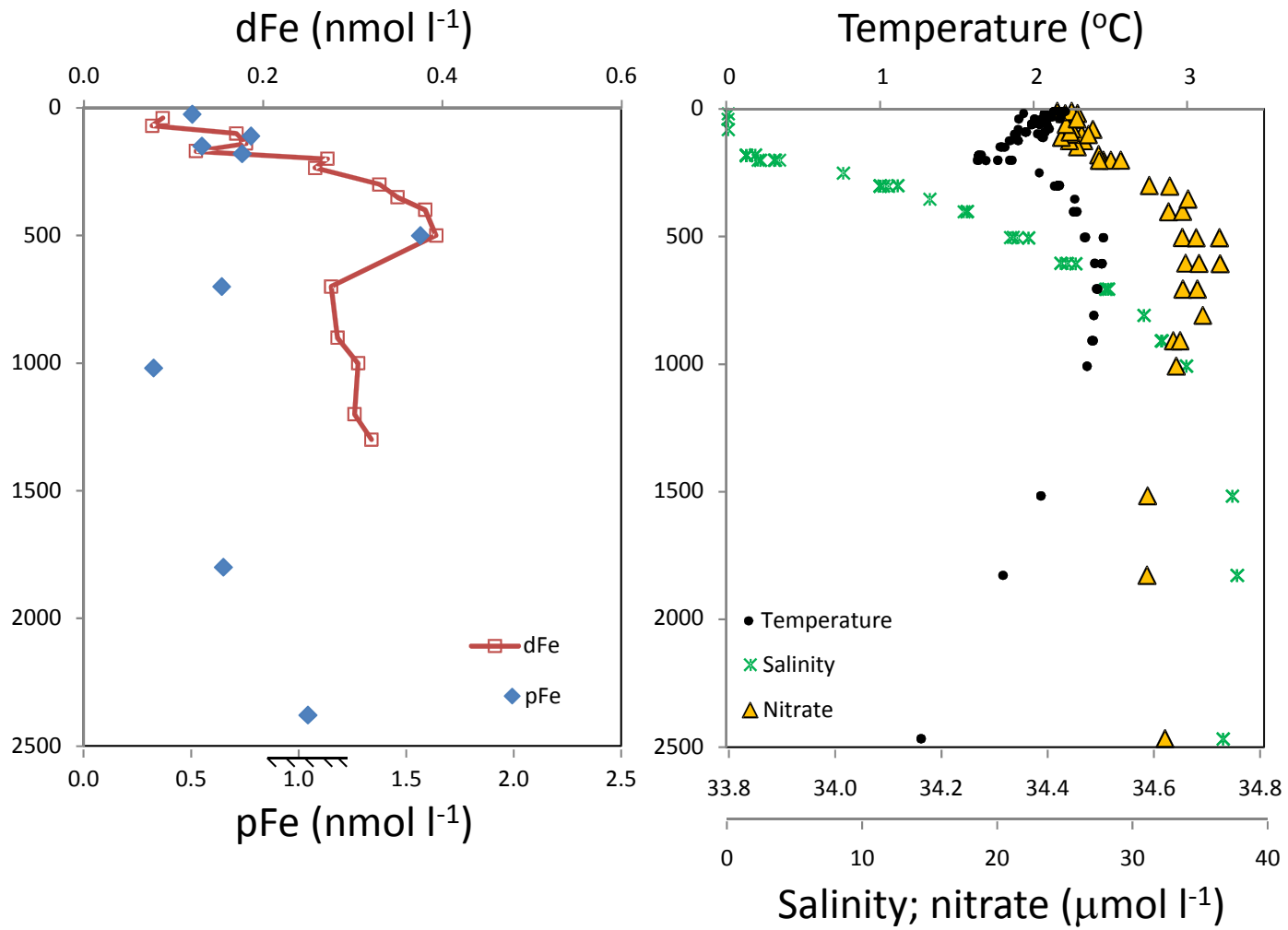


Figure 3b

### A3-1 (plateau)

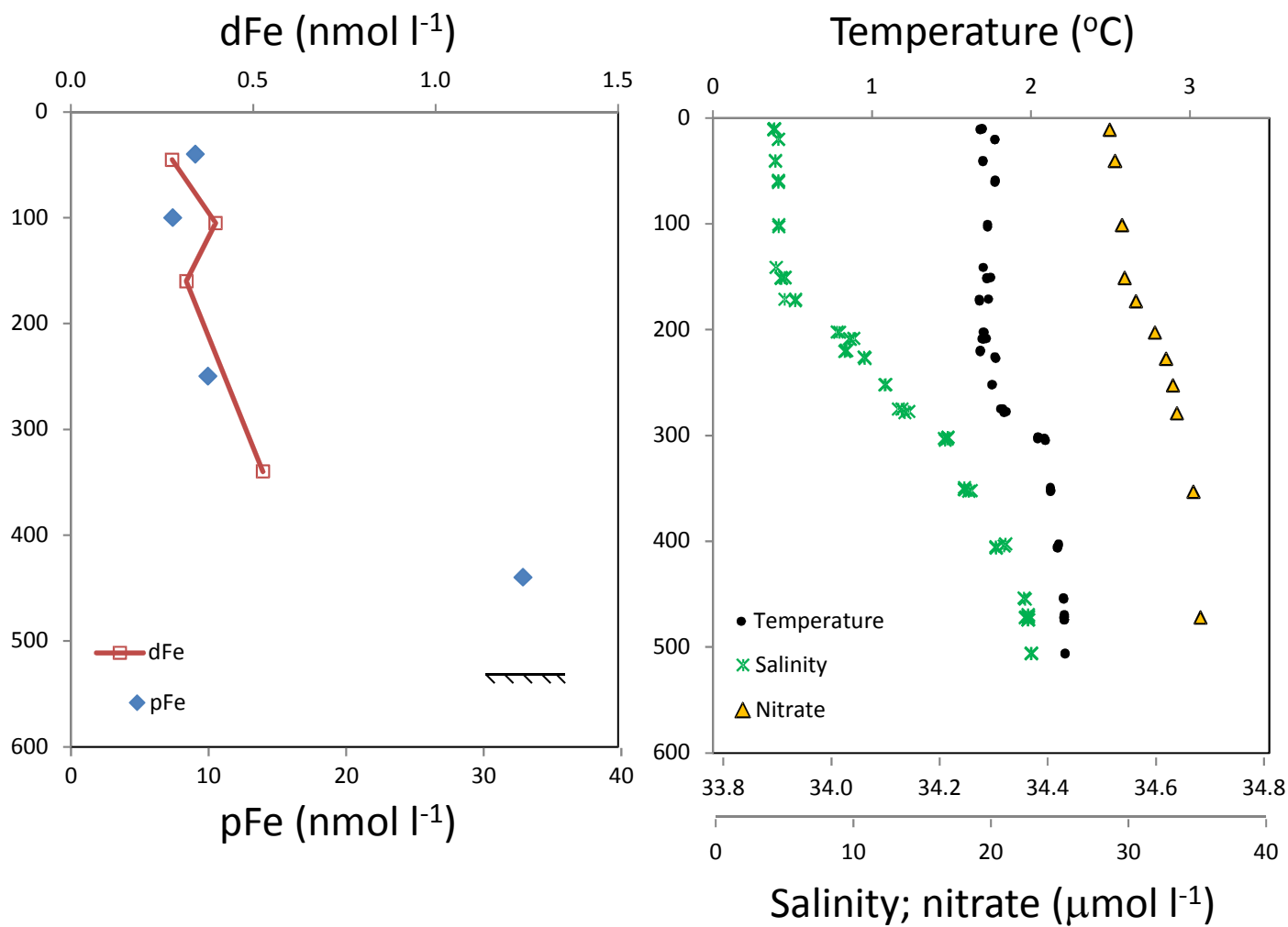


Figure 3c

### A3-2 (plateau)

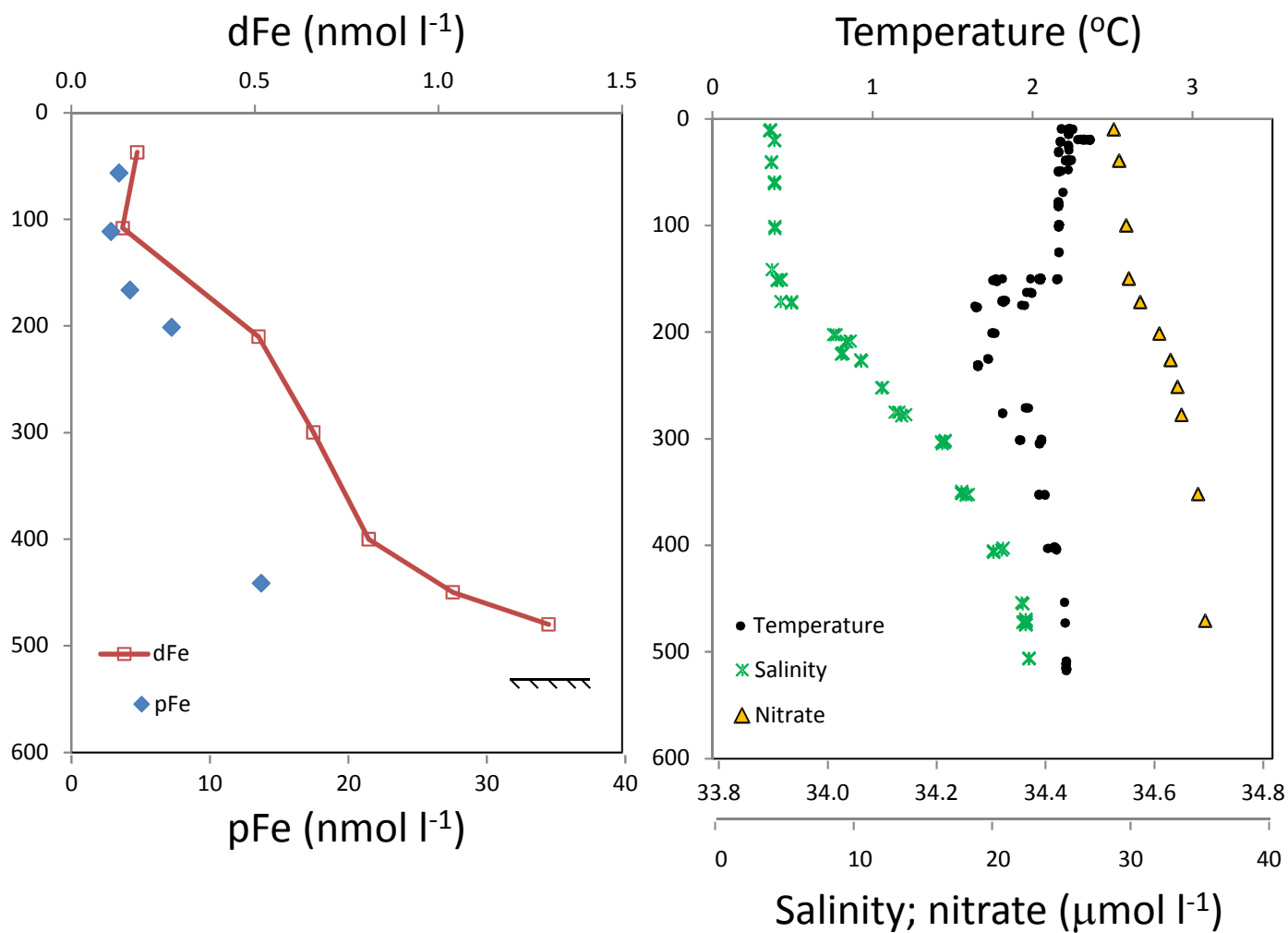


Figure 3d

### E-1 (plume)

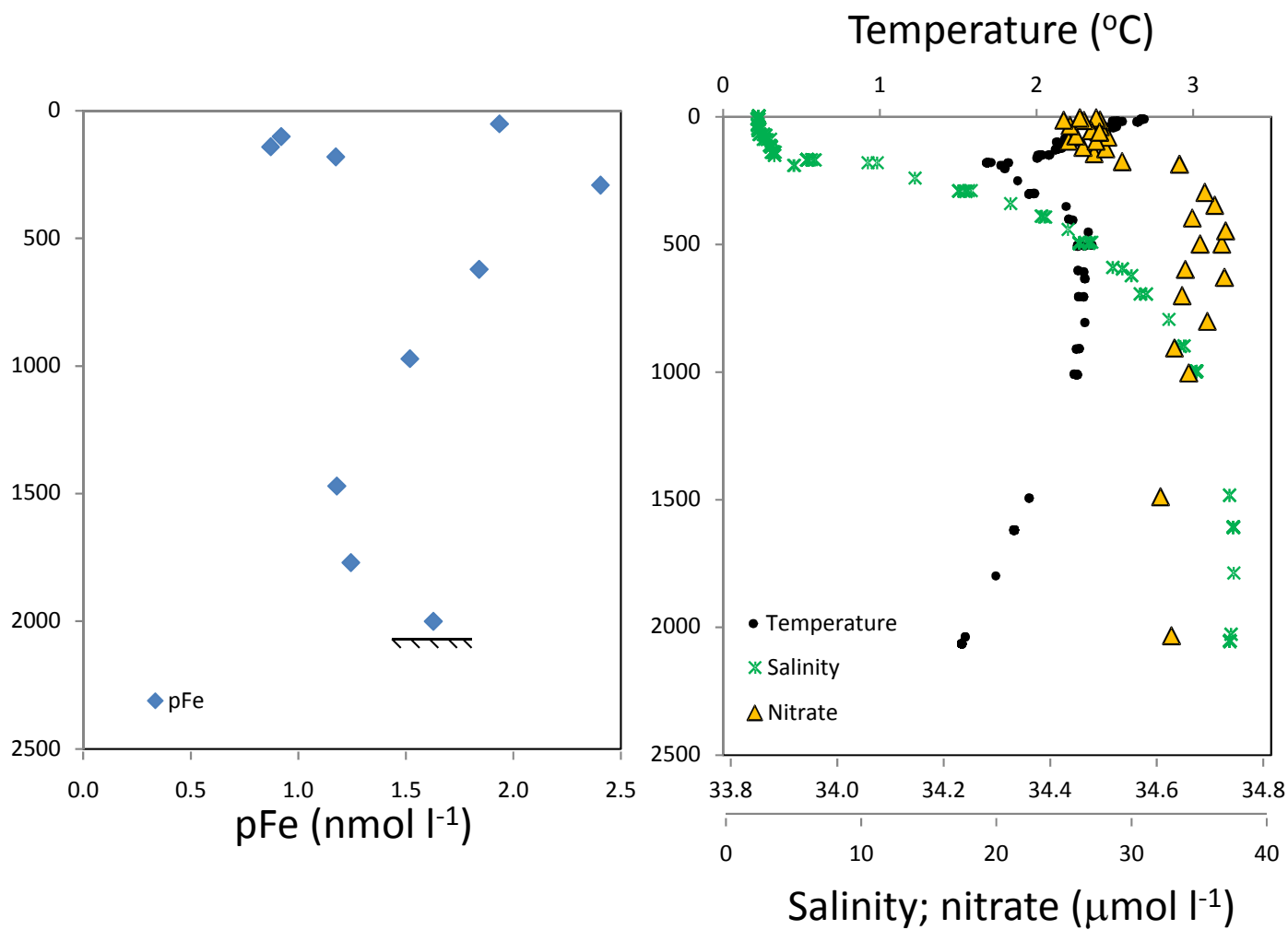


Figure 3e

E-3 (plume)

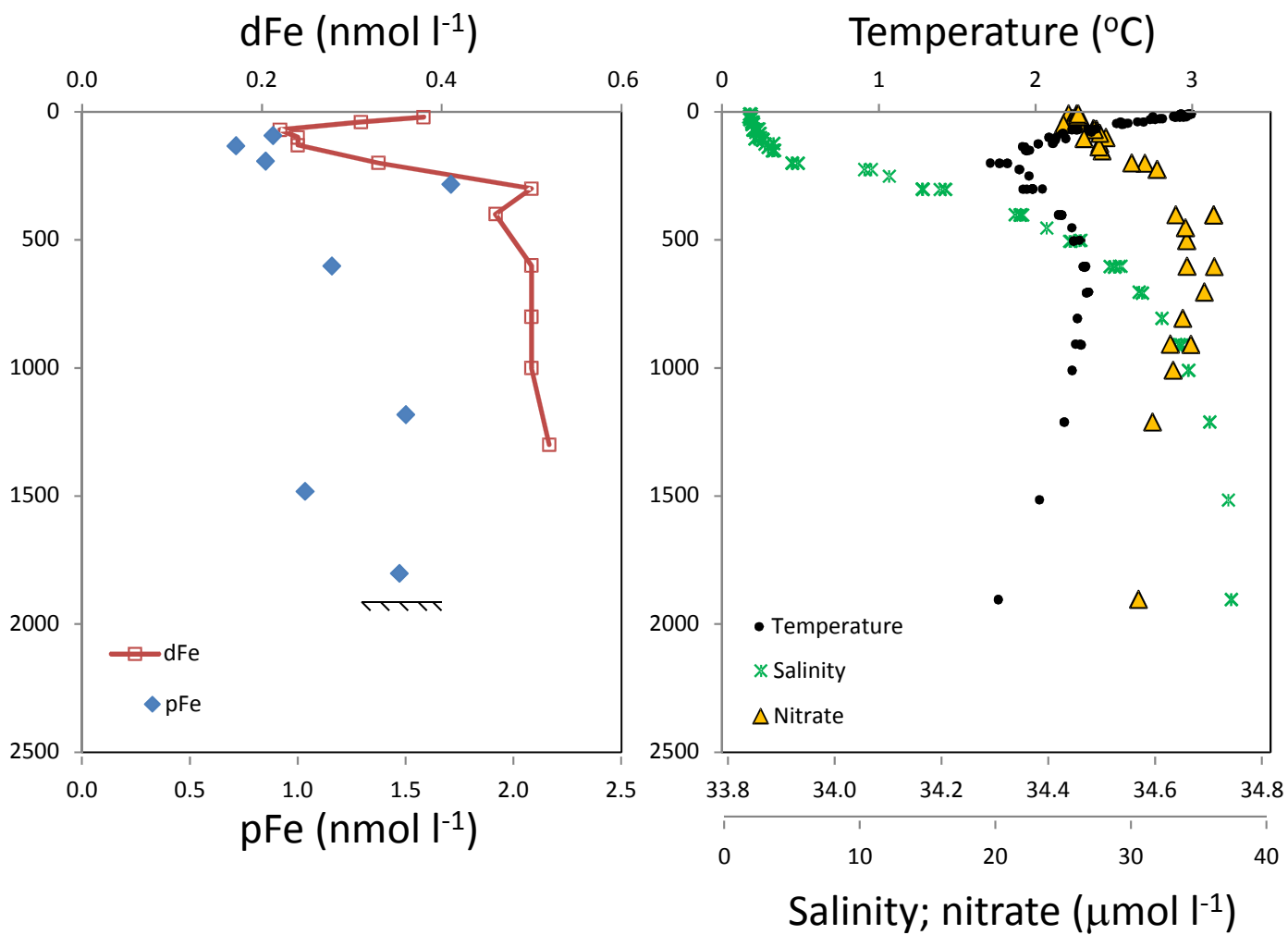


Figure 3f

### E-5 (plume)

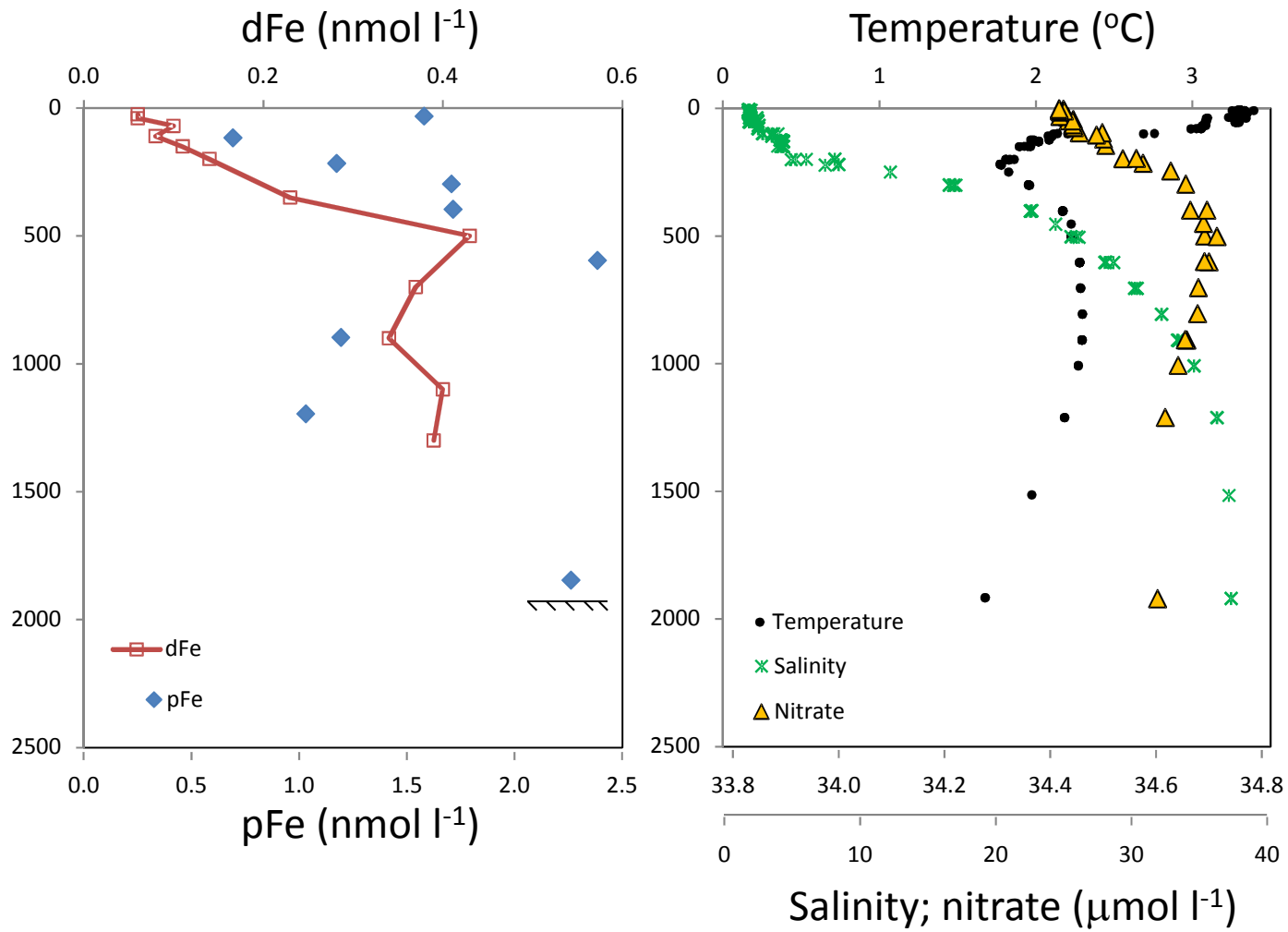




Figure 4a

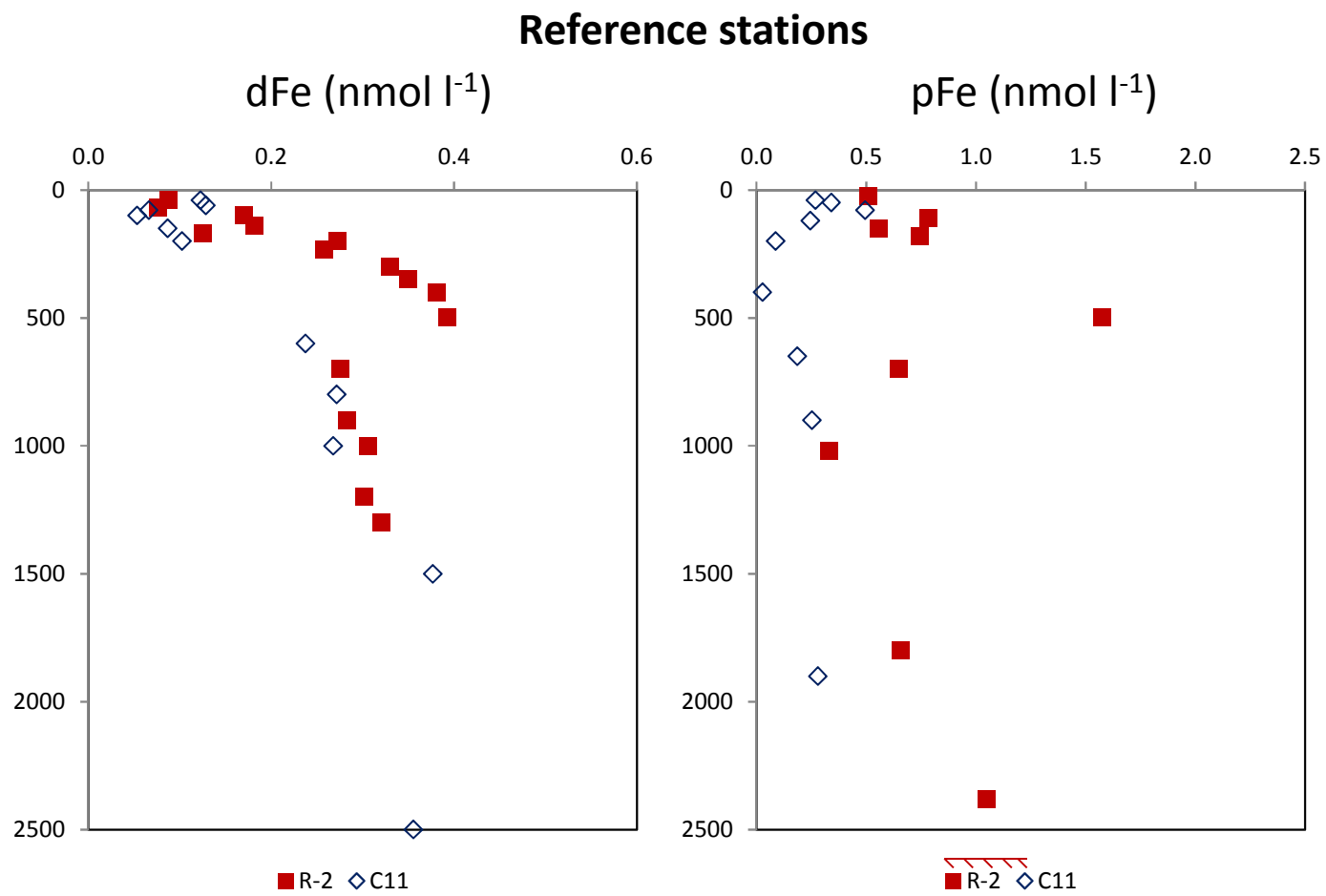


Figure 4b

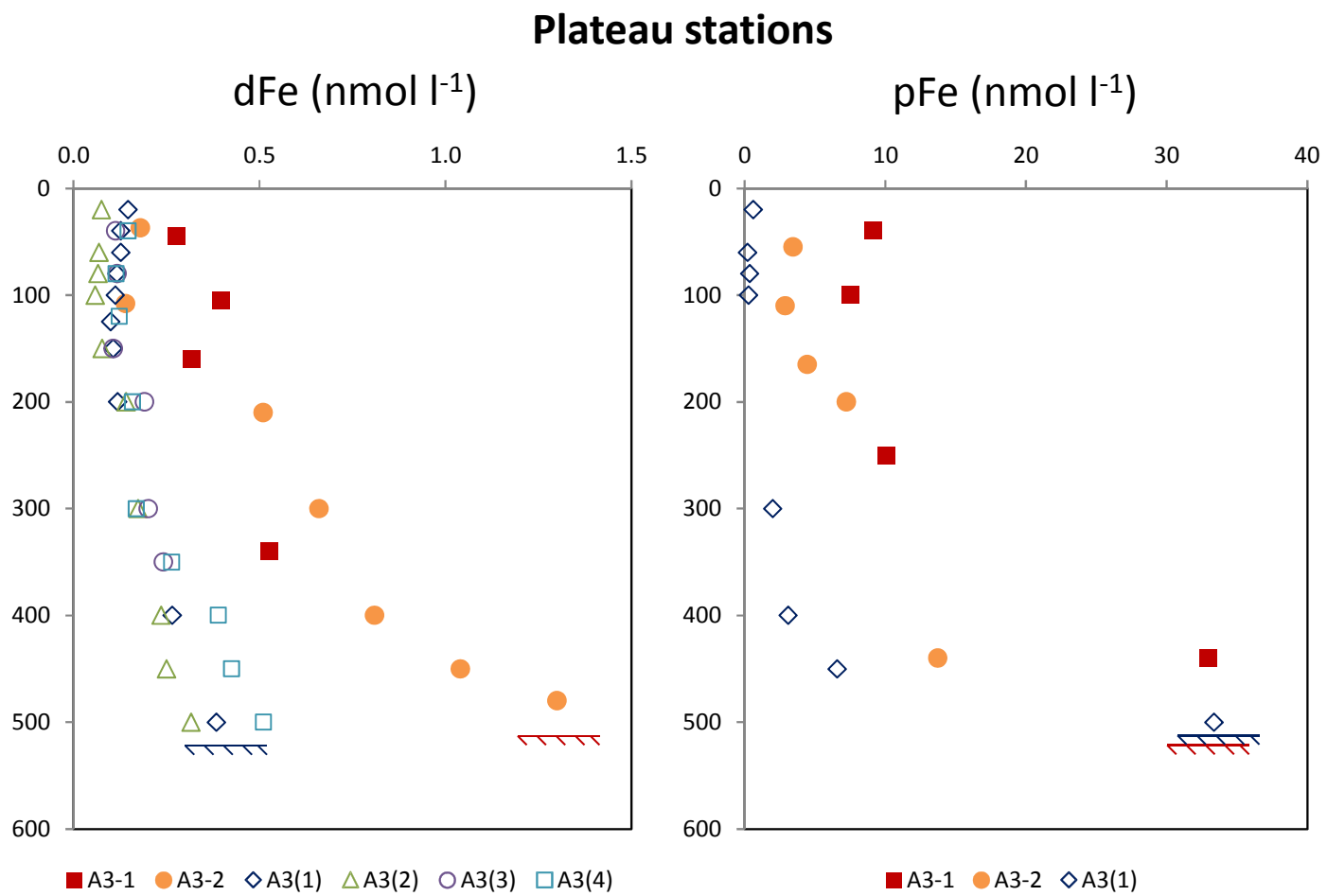


Figure 5

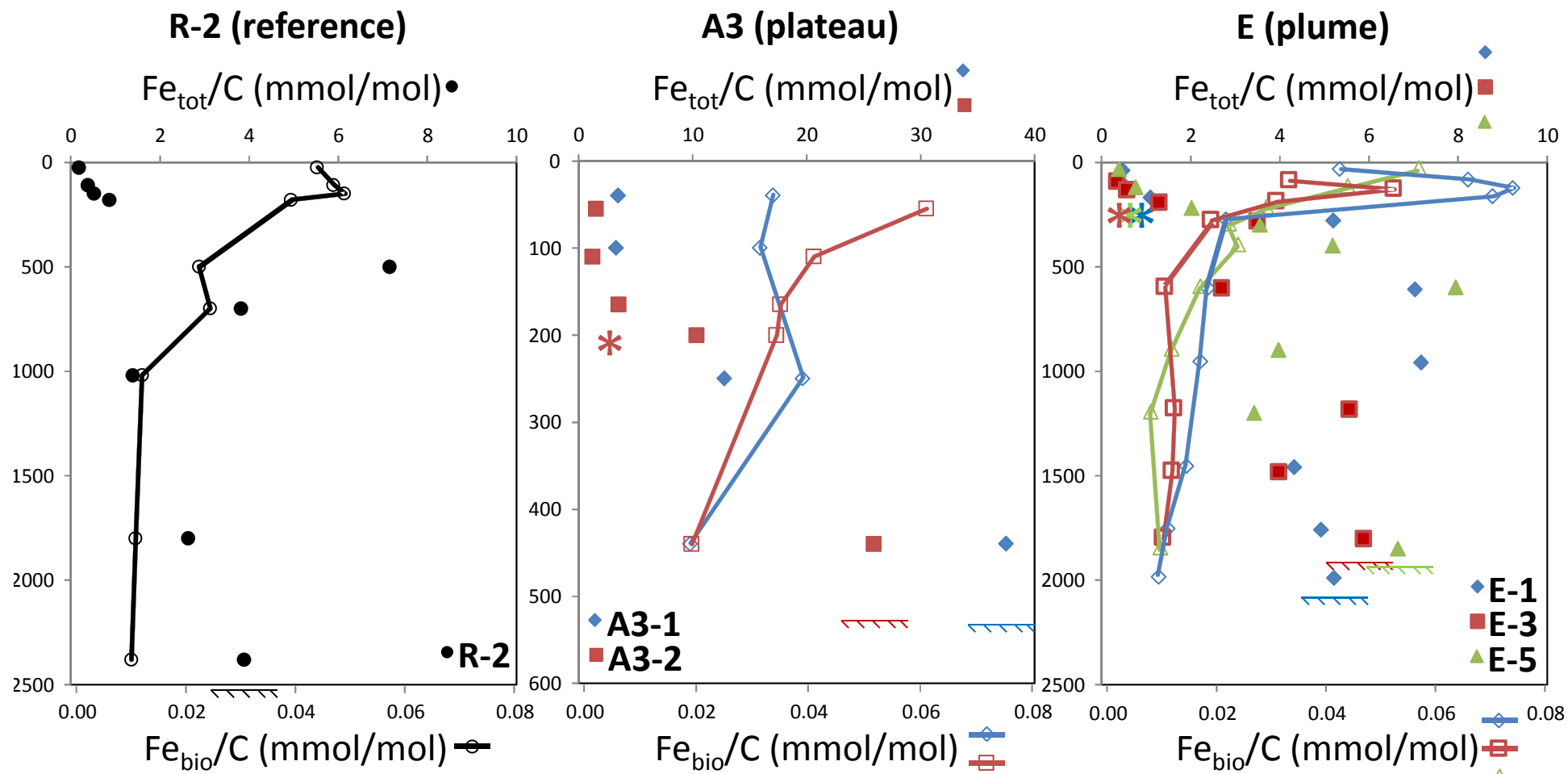


Figure 6

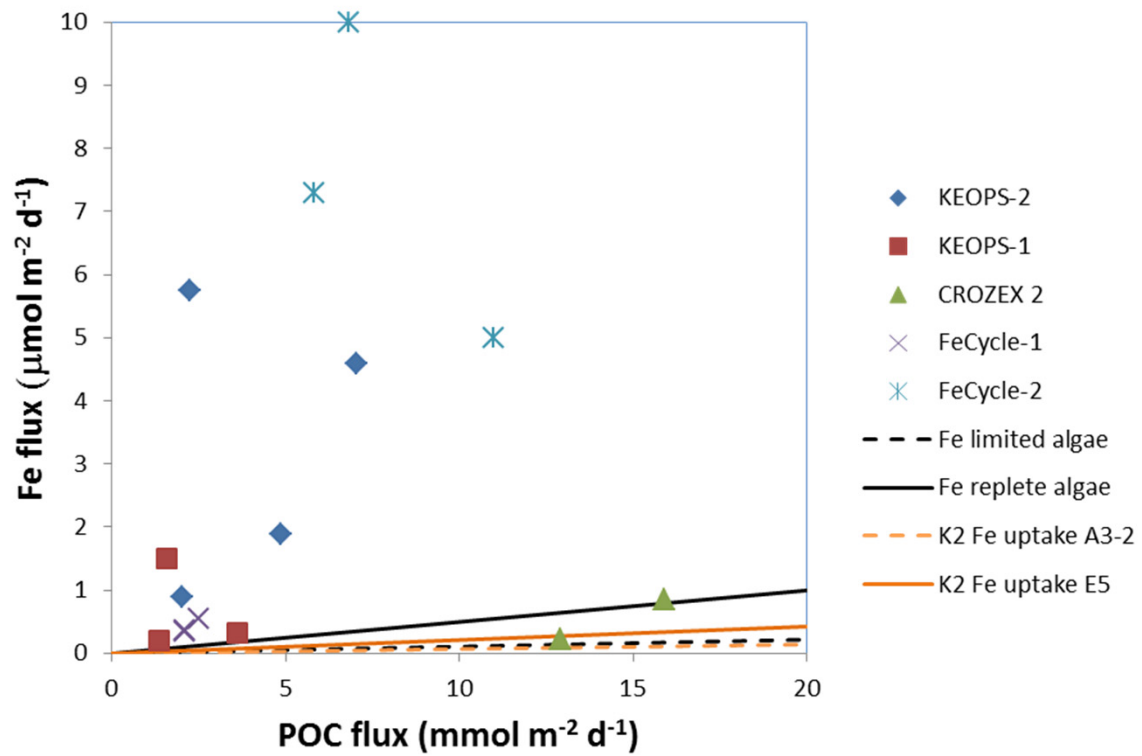


Figure 7a

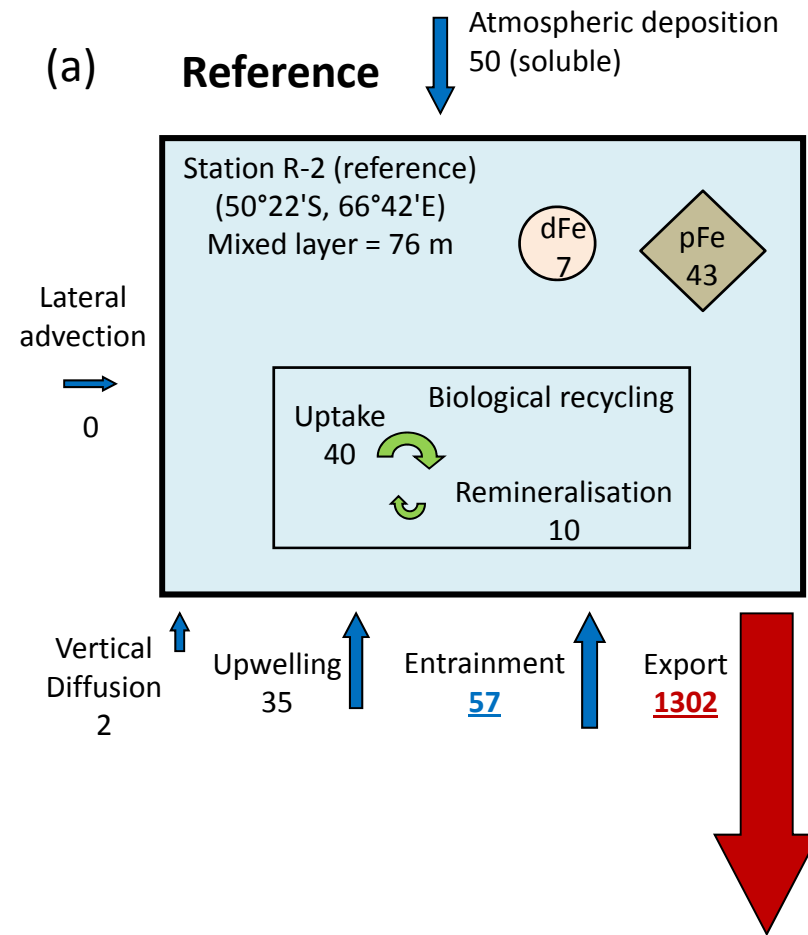


Figure 7b

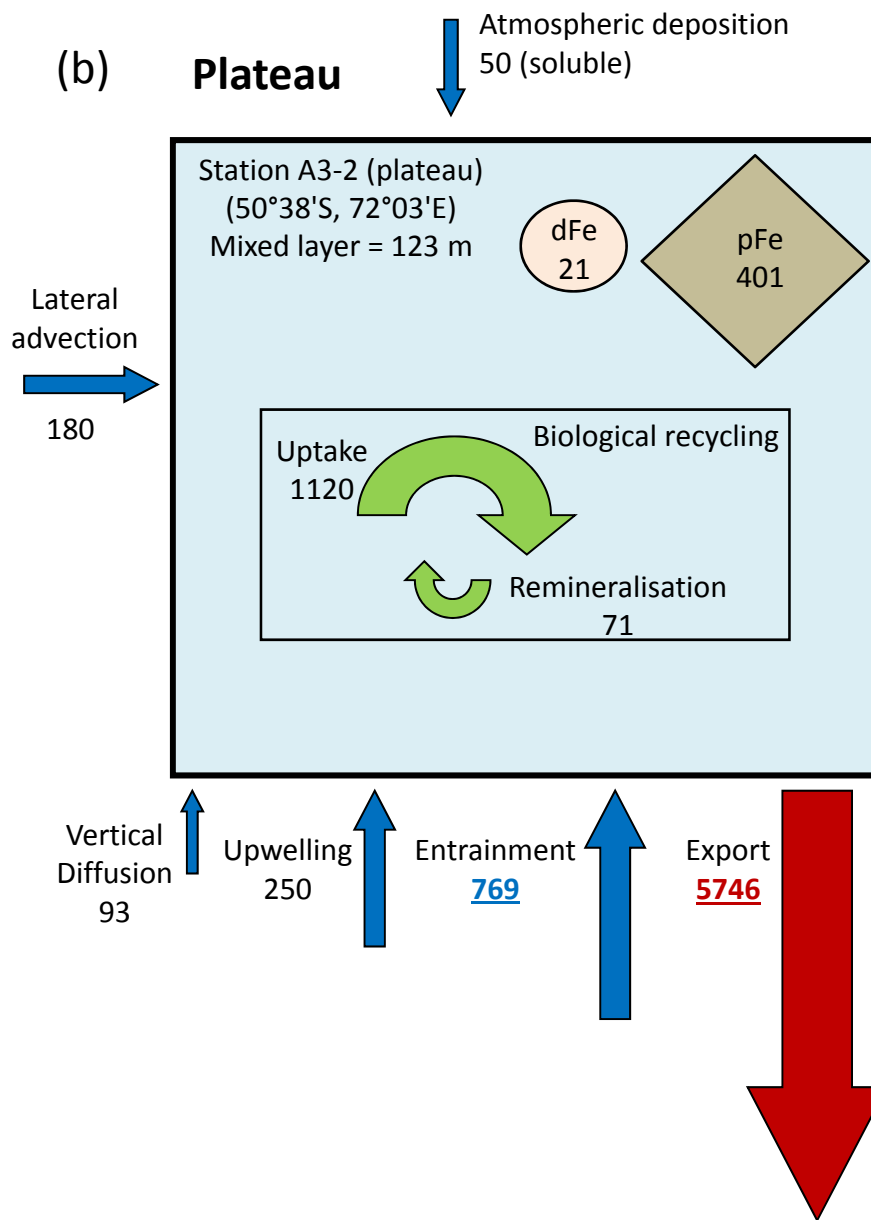


Figure 7c

